Very Forward Region
and
Polarisation

Konrad Elsener (CERN)
CDR Review Manchester
18-20 October 2011

Part I. Very Forward Region

(closely linked to the Machine Detector Interface sections of CDR Vol. 1)

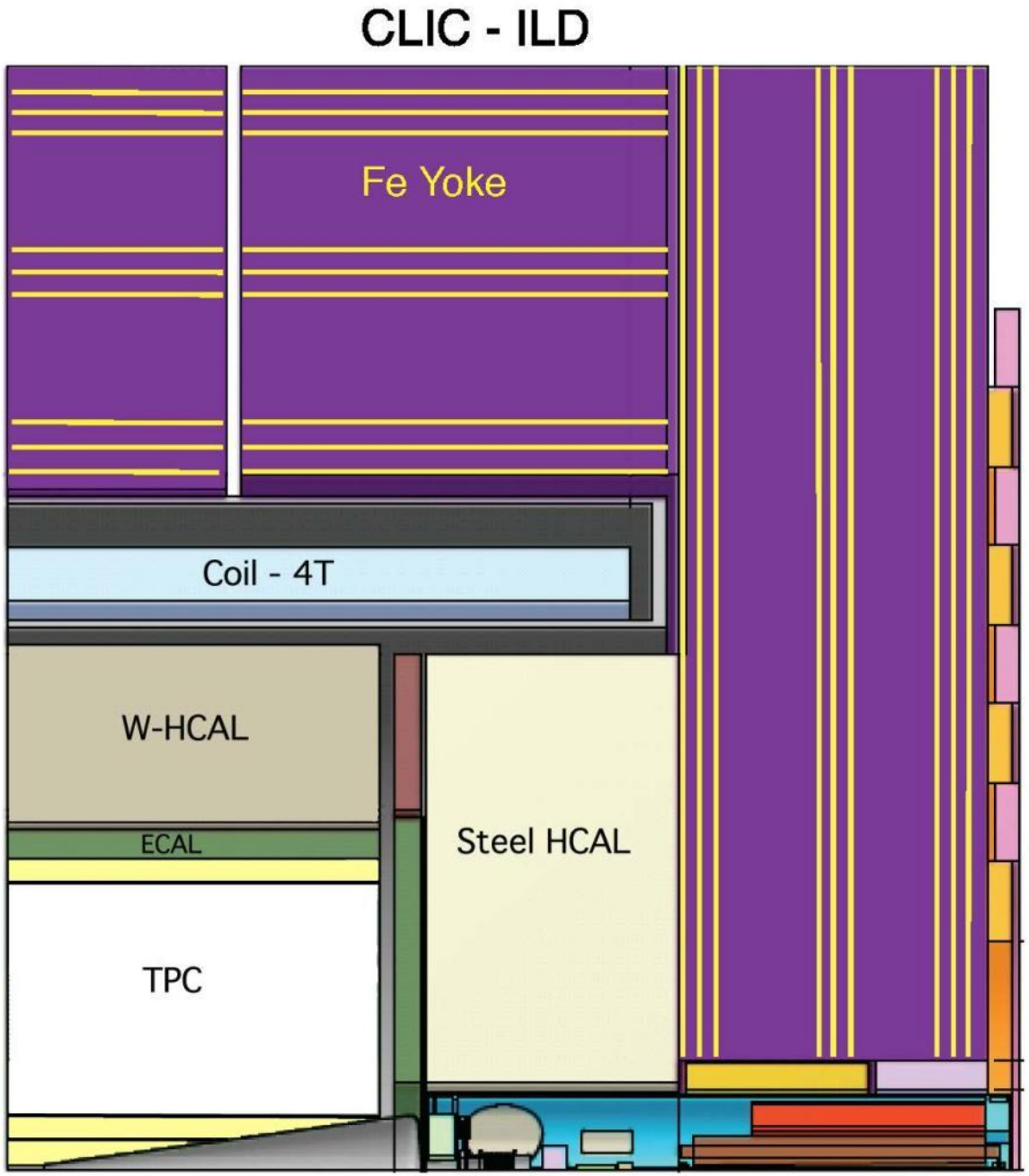

Fig. 3.1

Physics and Detector Aspects

-> close the forward detector acceptance
(ECal endcap -> LumiCal -> BeamCal)

110->38 46->10 mrad

centred on outgoing beam axis

-> precision luminosity measurement
(LumiCal)

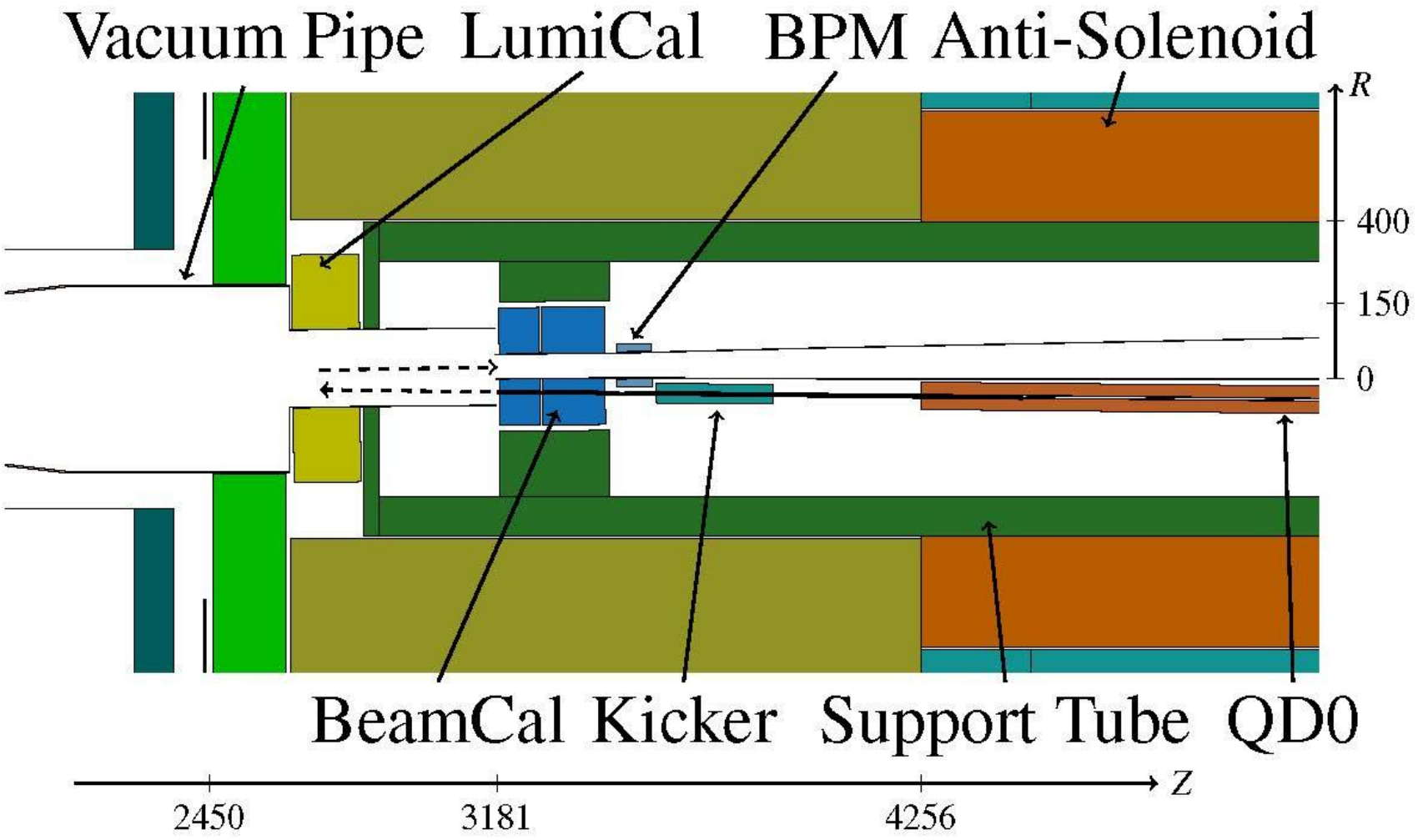

Fig. 3.3 – very forward region as in the GEANT4 simulation (CLIC_ILD)

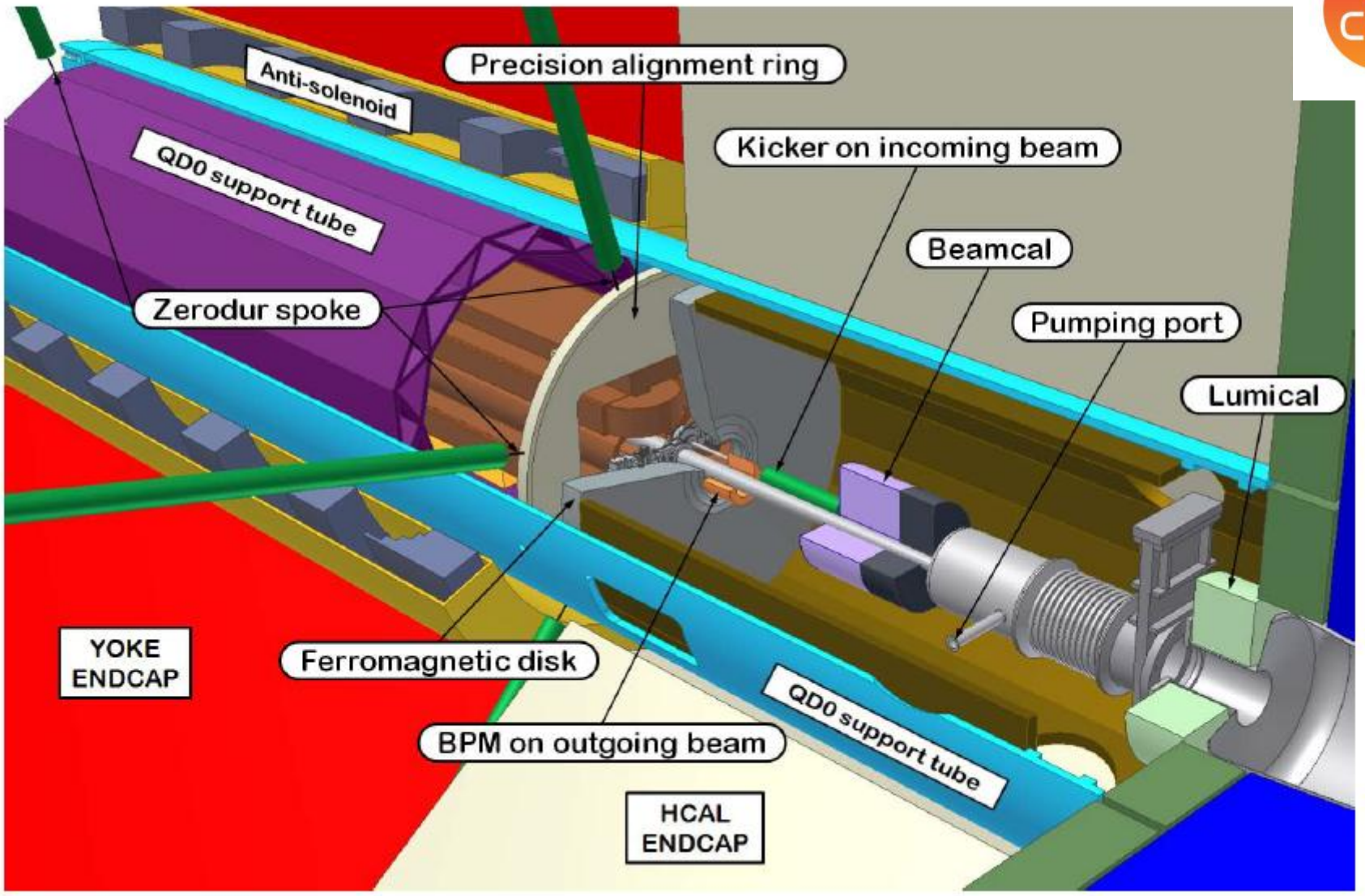

Fig. 11.13 – very forward region as in the engineering model (CLIC_SiD)

Beam / Accelerator Aspects -> cf. CDR Vol. 1

-> final focusing and orbit – alignment, stability
(QD0 and anti-solenoid;
QD0 mechanical support)

-> intra train feedback

(mostly) not in the scope of the present CDR review

QD0 stabilisation - 0.15 nm above 4 Hz

- compact detector/tunnel design (cf. H. Gerwig)
- ring chicane shielding (cf. H. Gerwig)

-> CDR Vol. 1

- support QD0 from a pre-isolator in the accelerator tunnel
- choose hybrid solution for QD0 (perm. magnet, little cooling)
- two-in-one support tube for QD0 and very forward calorimeters
- active stabilisation system below QD0

LumiCal and BeamCal

Synergies with ILC, collaboration in FCAL

LumiCal – measure luminosity using Bhabha events

(NB. luminosity spectrum measurement using large-angle Bhabha scattering, not treated here)

located at z=2.6 m
geometrical acceptance: 38-110 mrad
fiducial acceptance: 44 – 80 mrad
-> 62 pb at 3 TeV
-> statistical accuracy
for 500 fb^{-1}: 1.8×10^{-4}

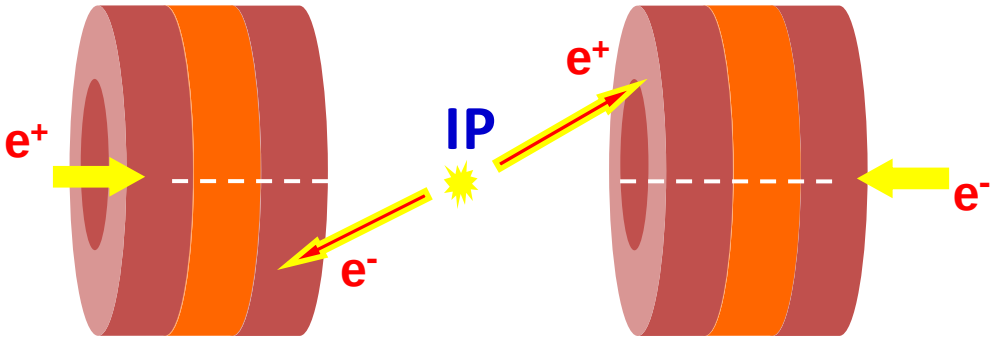

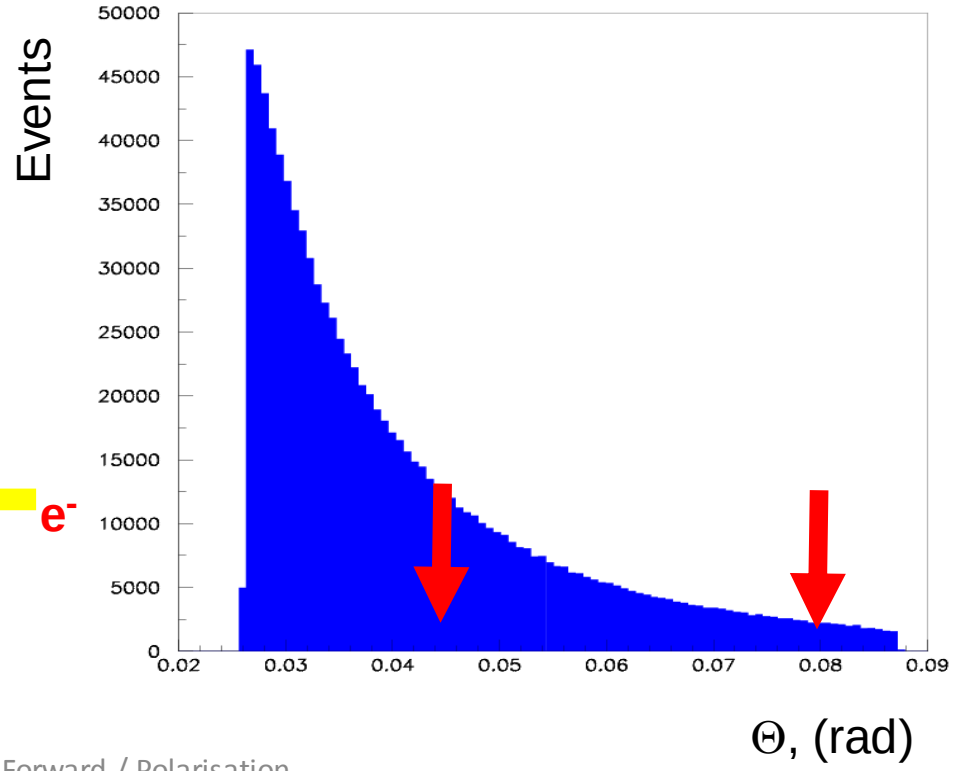

LumiCal – preliminary design (FCAL collaboration)

In CLIC_ILD:
located at z=2.6 m
total depth: 171 mm
inner radius: 100 mm
outer radius: 290 mm

40 layers:
- 3.5 mm W plates
- 320 μm Si sensors
- 550 μm connectivity

readout electronics
at outer radius

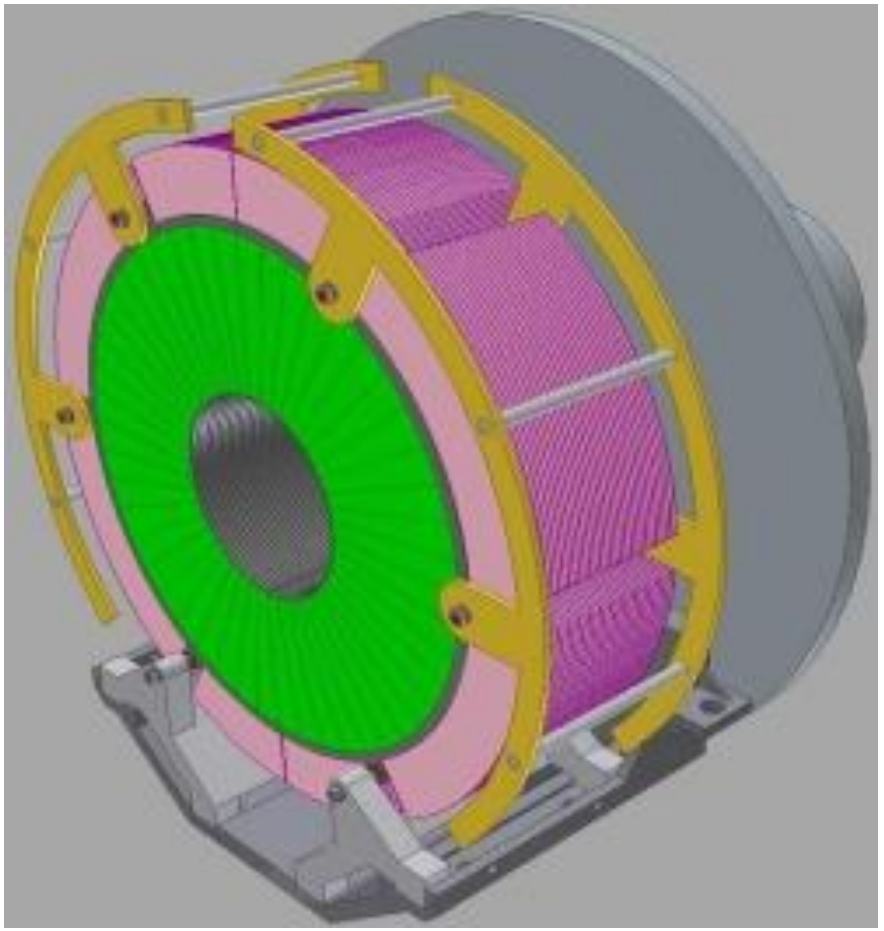

Fig. 9.3

LumiCal – sensors (FCAL collaboration)

Sensors pads CLIC:
(preliminary)
48 divisions azimuthally
50 divisions radially (ILC: 64)

(prototype silicon sensors
From Hamamatsu)

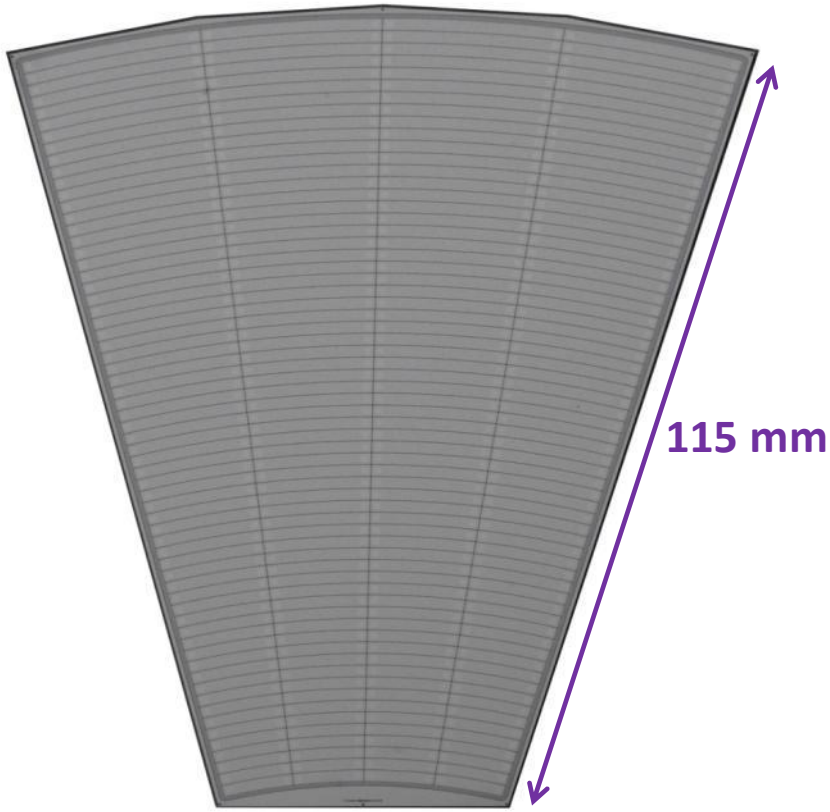

LumiCal – sensors (FCAL collaboration)

Sensors pads CLIC:
(preliminary)
48 divisions azimuthally
50 divisions radially (ILC 64)

(ILC LumiCal sensor:
test beam set-up
August 2011)

LumiCal – accuracy (systematics!)

ILC at 500 GeV: requiring 0.1% accuracy

high statistics physics channels at 500 GeV, e.g. e+e- -> WW or f f
yield approx. 10^6 events for 500 fb^{-1}
-> statistical error 10^{-3}

-> LumiCal accuracy should be the same or better

CLIC at 3 TeV: requiring 1% accuracy

(requires e.g. 0.2 mrad or 0.5 mm accuracy on inner edge of LumiCal)
decided in February 2009, at start of first simulations studies
considered sufficient (?) w.r.t. statistics in typical physics processes
considered realistic for CLIC (higher background!)

LumiCal – issues

Background -> cf. A. Sailer's talk

systematic errors -> **studies in progress**
several contributions "ok.", similar to ILC;
background and beam-beam effects: **pending**

very compact design, ambitious -> connectivity ?

NB. LumiCal simulation studies to be repeated after CDR, review required accuracy, pad sizes, 40 layer depth etc.

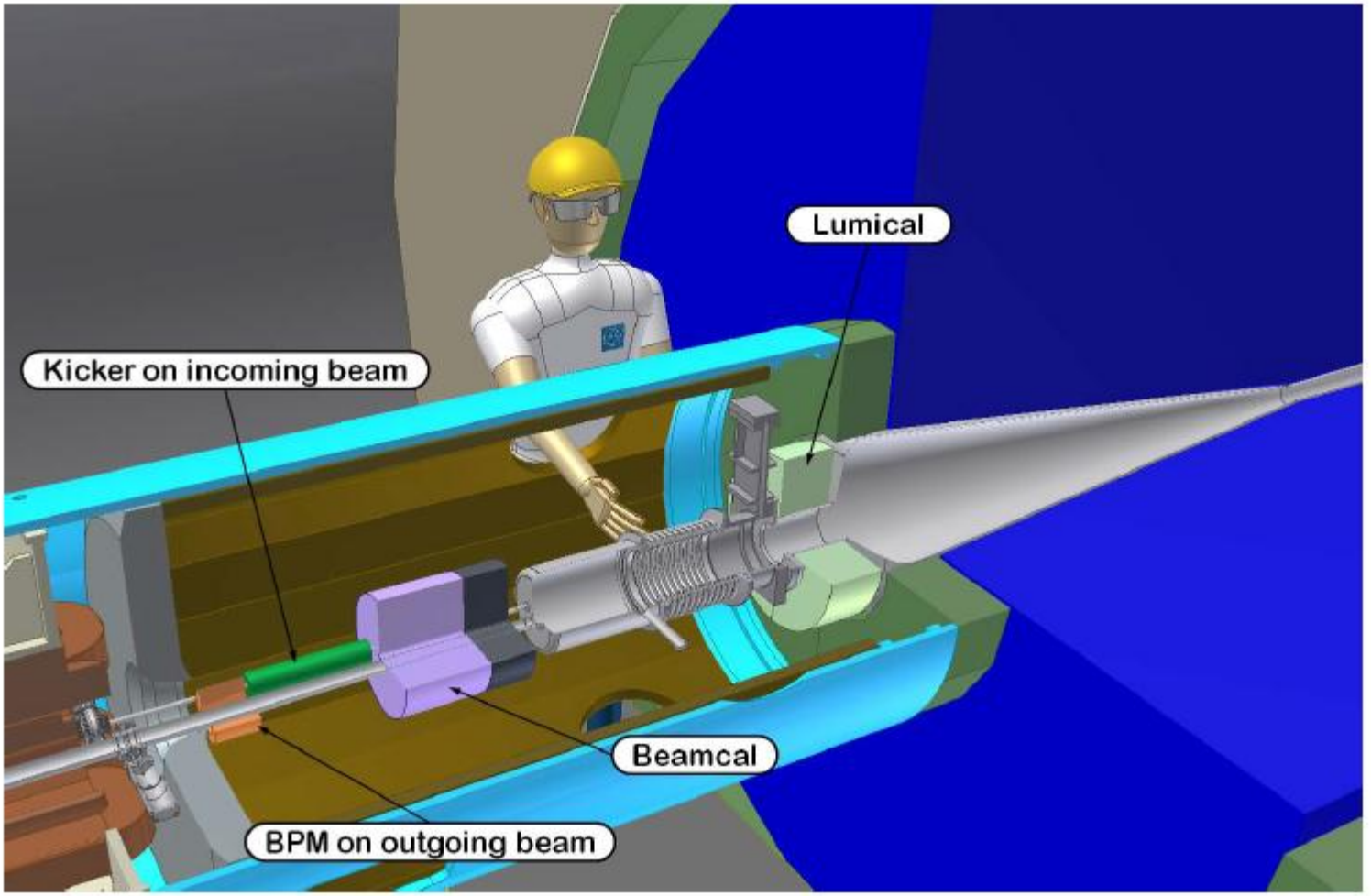

Fig. 11.15: Support tube with QD0, BPM and kicker, vacuum valve and BeamCal

BeamCal – tag h.e. electrons at small angles

(possibly used to give feedback to beam steering – not studied)

In CLIC_ILD:

located at z=3.1m

total depth: 260 mm (w/graphite)

inner radius: 32 mm

outer radius: 150 mm

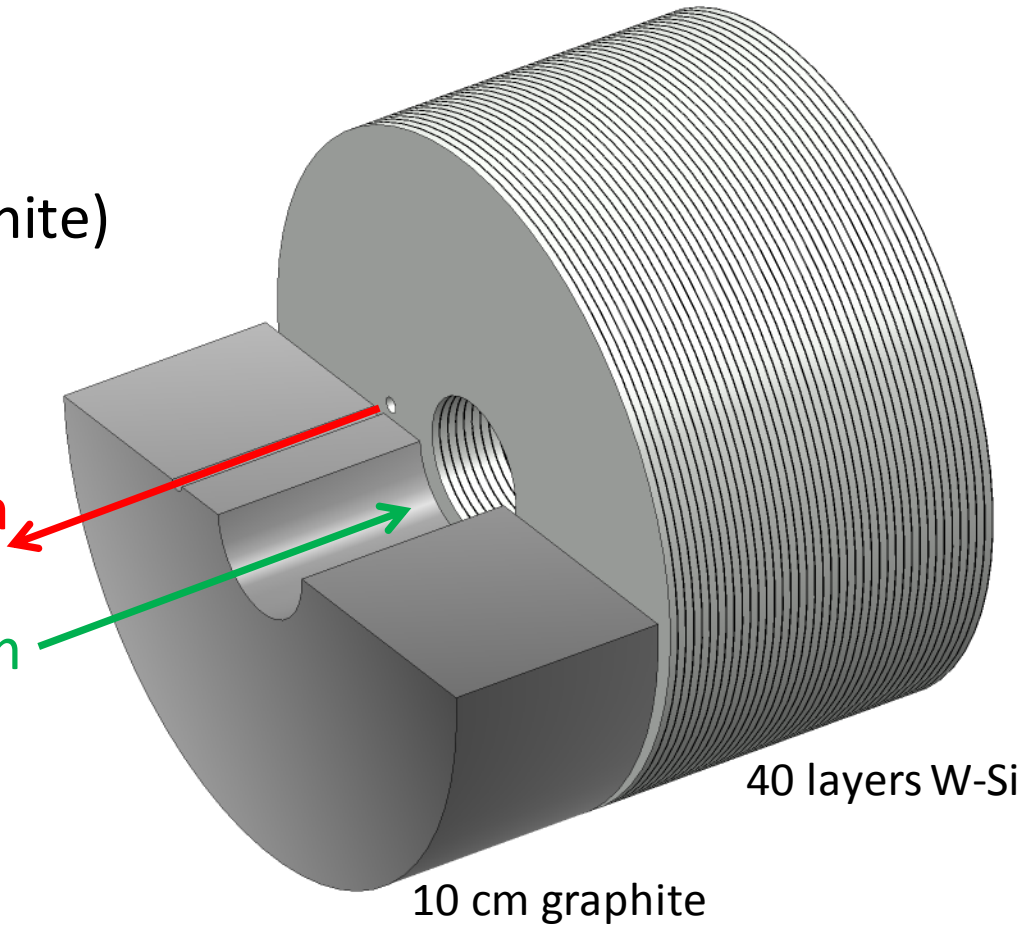

40 layers:

3.5 mm W plates

+ sensors

BeamCal – a single h.e. electron and 10 BX of bg.

(shown here: energy deposition in the 10th layer)

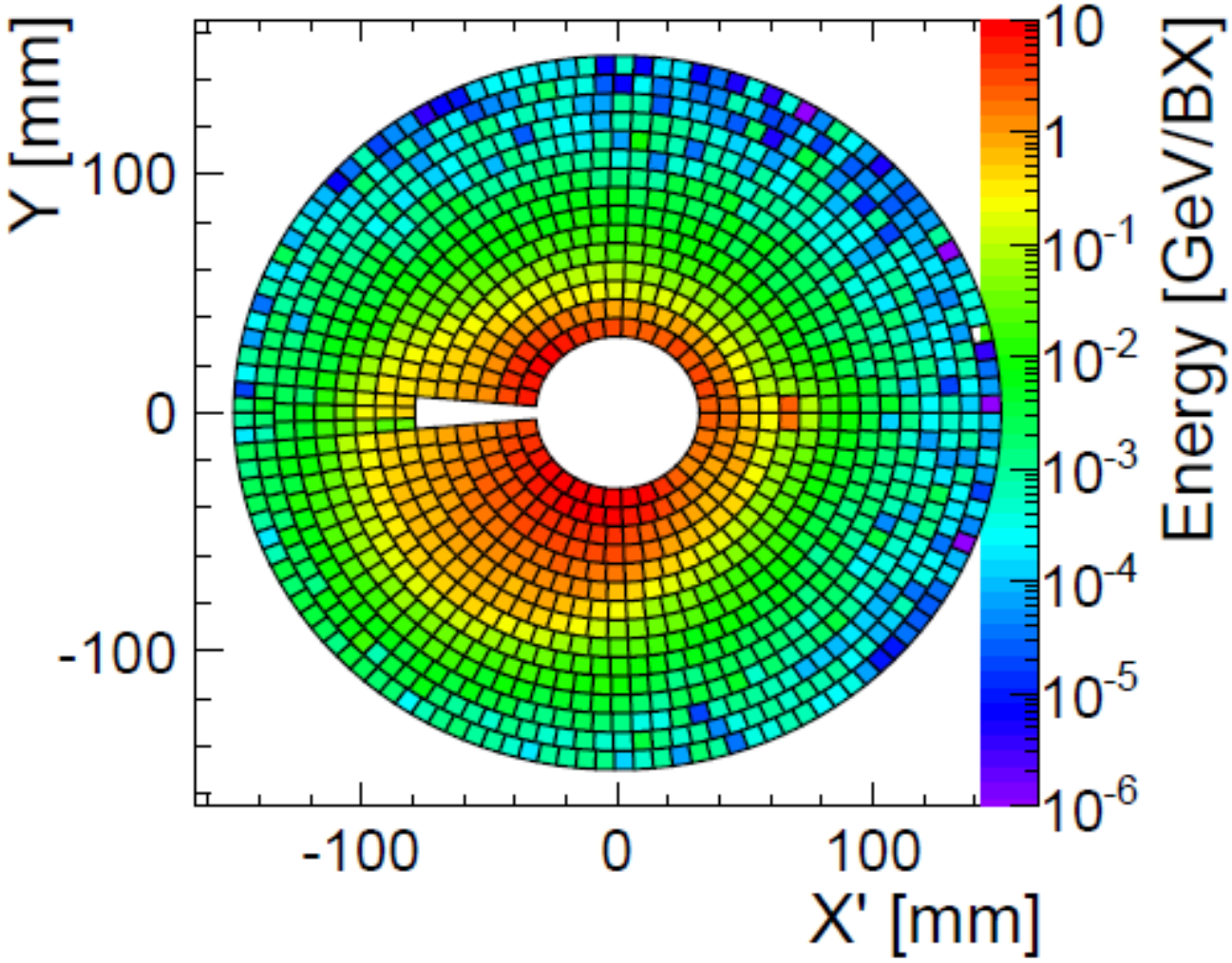

Fig. 9.6

BeamCal – issues

radiation damage to sensors
-> cf. FCAL work on GaAs, diamond sensors

very high occupancy (-> readout electronics)

efficiency to tag h.e. electrons w/background:
simulation studies **pending**

Part II. Polarisation

(not yet in CDR Vol. 2)

SYNERGY WITH ILC

From CLIC CDR Vol. 1 (Accelerator):

Polarisation as **produced**, transported to the IP:

CLIC baseline design:

-> electrons polarised, **80%**

-> positrons unpolarised

CLIC possible upgrade:

-> positrons polarised

From CLIC CDR Vol. 1 (Accelerator):

Polarisation **measurement** in the $B_{eam}D_{elivery}S_{ystem}$ and beyond:

CLIC baseline design:

-> analogous to ILC: Compton backscattering from laser beam (polarimeter in BDS);
assume polarimeter accuracy of 0.3% (cf. ILC)

No polarimeter in the post-collision line (i.e.. after IP) !

(strong beam-beam effects -> $3x10^8$ coherent pairs / BX
-> too much background after the IP)

-> rely on spin tracking calculations through 700m of BDS

Depolarisation at the IP – important at 3 TeV:

various recent papers –
luminosity weighted depolarisation found to be approx. 3 - 5%

What is the uncertainty of such a calculated depolarisation ?

Cf. D. Schulte:
depolarisation is less pronounced at the high-energy end of the luminosity spectrum

from D.Schulte - Polarisation

Not yet in CDR

No detailed integrated studies
- but some considerations/calculations
- e.g. figure eight turn-around for electrons
- depolarisation in IP (GUINEA-PIG++)

Expect >80% electron polarisation at source
- 87% have been demonstrated at SLAC

No polarised positrons in baseline
- could use ILC helical undulator source
- but have other options

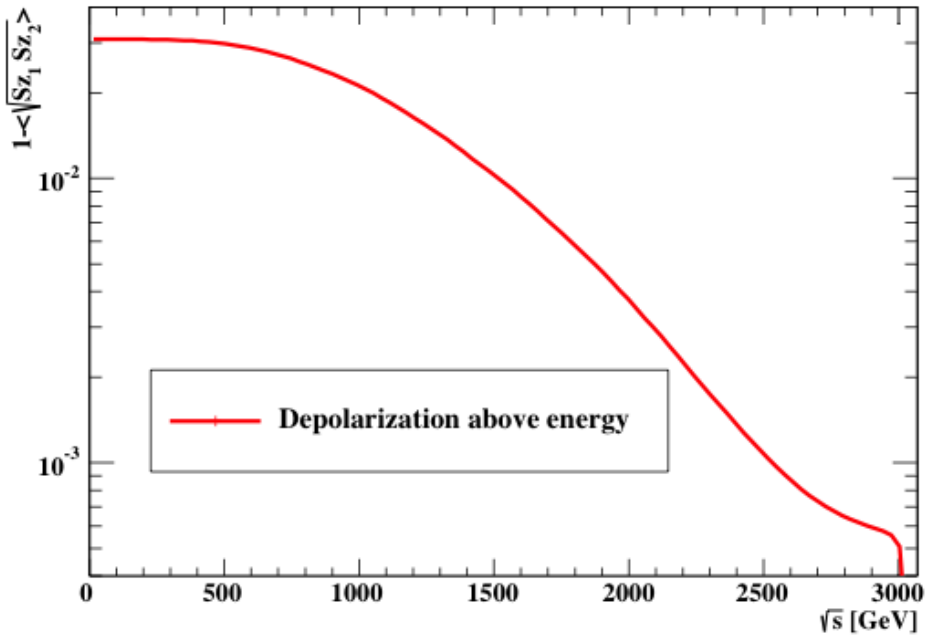

J. Esberg, preliminary

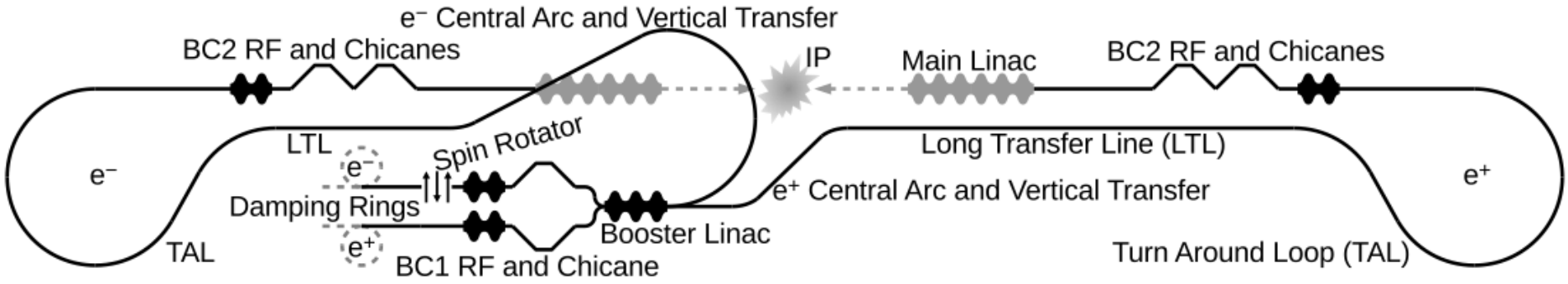

Plans for CDR Vol. 2 – Dec 2011:

Insert a section into chapter 1 (physics potential)
describing the benefits of polarisation in

a) chargino-neutralino benchmark channel
b) Z' at 10 TeV

assuming "ad hoc" accuracy of polarisation

longer term:
assess accuracy of polarisation (vs. depolarisation);
investigate measuring the "effective polarisation"
via physics channels, **e.g. WW production, single W prod.**

Spare Slides Part I (VF)

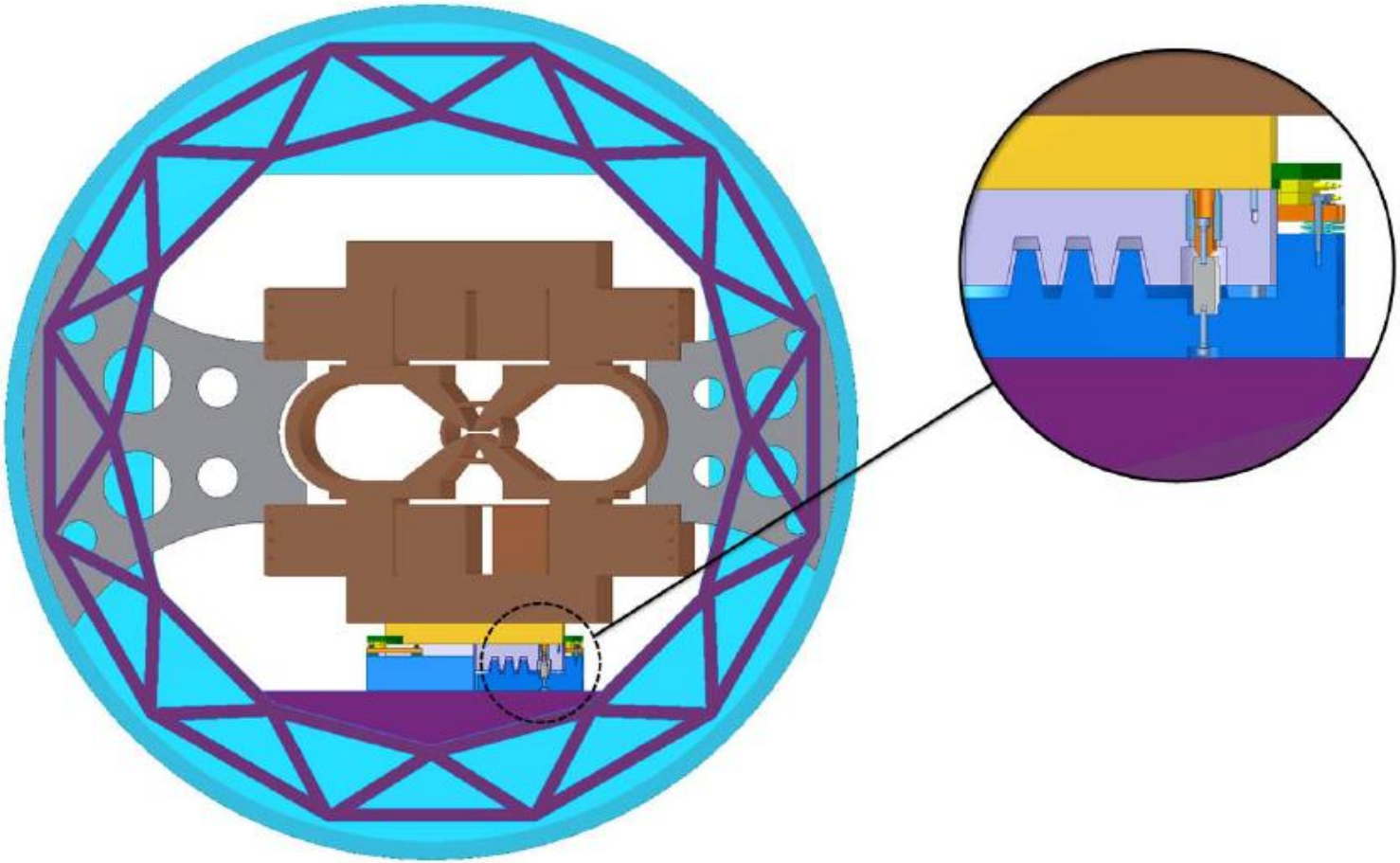

Fig. 11.16: QD0 support detail, copper coils are supported by outer tube. The active stabilisation system is shown in the insert.

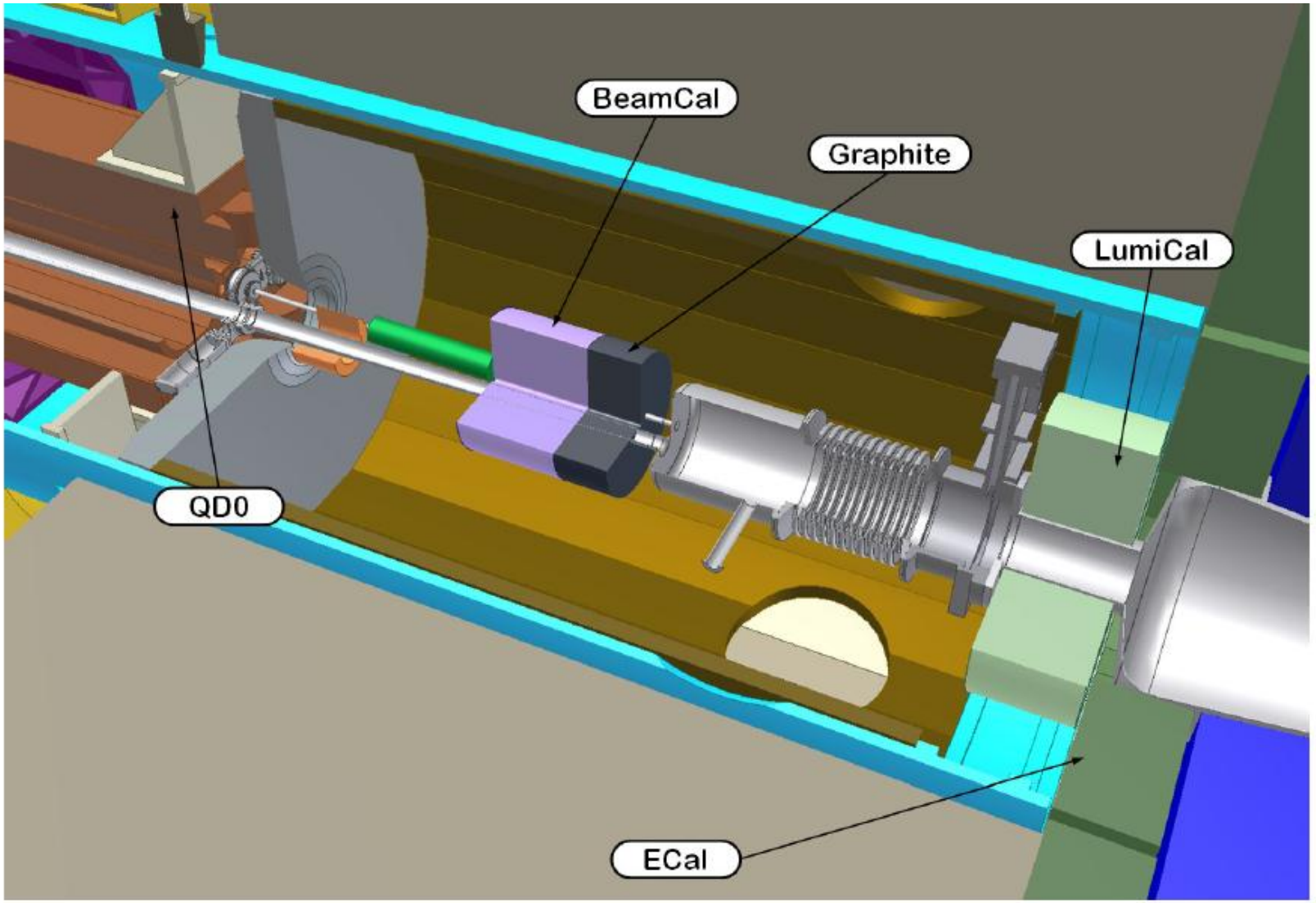

Fig. 9.3

PUBLISHED BY IOP PUBLISHING FOR SISSA

RECEIVED: *September 15, 2010*
ACCEPTED: *November 12, 2010*
PUBLISHED: *December 7, 2010*

Forward instrumentation for ILC detectors

Table 1: The estimated systematic uncertainties on the luminosity measurement from all sources considered above at a centre-of-mass energy of 500 GeV.

Source	Value	Uncertainty	Luminosity Uncertainty
σ_θ	2.2×10^{-2}	100%	1.6×10^{-4}
Δ_θ	3.2×10^{-3}	100%	1.6×10^{-4}
$a_{\rm res}$	0.21	15%	10^{-4}
luminosity spectrum			10^{-3}
bunch sizes σ_x, σ_z,	655 nm, 300 μm	5%	1.5×10^{-3}
two photon events	2.3×10^{-3}	40%	0.9×10^{-3}
energy scale	400 MeV	100%	10^{-3}
polarisation, e^-, e^+	0.8, 0.6	0.0025	1.9×10^{-4}
total uncertainty			2.3×10^{-3}

ILC 500 GeV
Cuts optimization

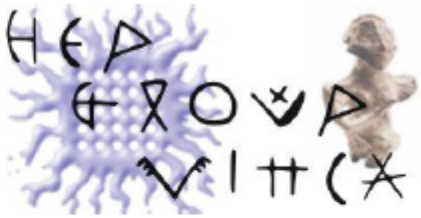

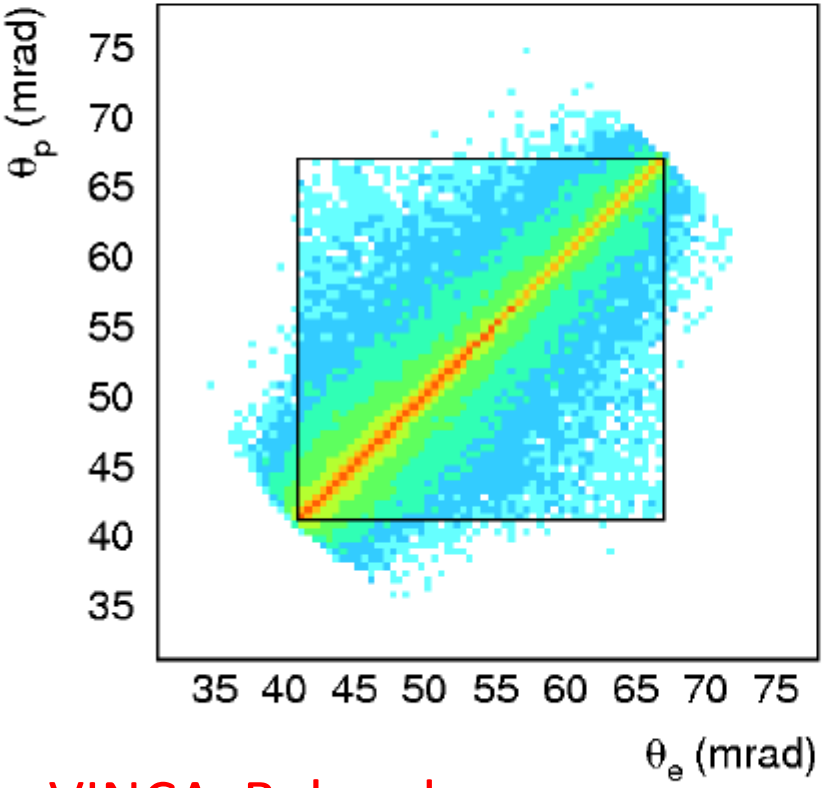

Most Bhabha events that migrate outside of the fiducial volume start out near the edges.

$\theta_e, \theta_p \approx \theta_{min}$
$\theta_e, \theta_p \approx \theta_{max}$

S. Lukic, VINCA, Belgrade

very first look
CLIC 3 TeV

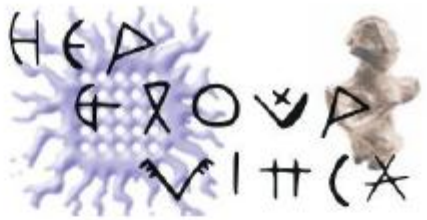

- BHSE 71 % (E_{rel} + fiducial volume, simulated with Gaussian beams) – difficult to reduce to zero
- Needs to be more reliably estimated and corrected

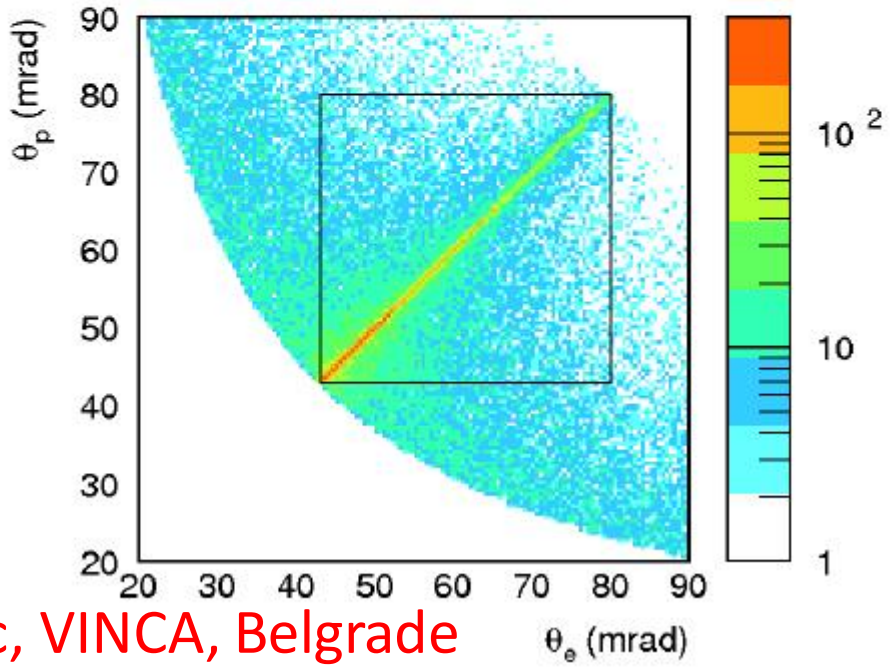

S. Lukic, VINCA, Belgrade

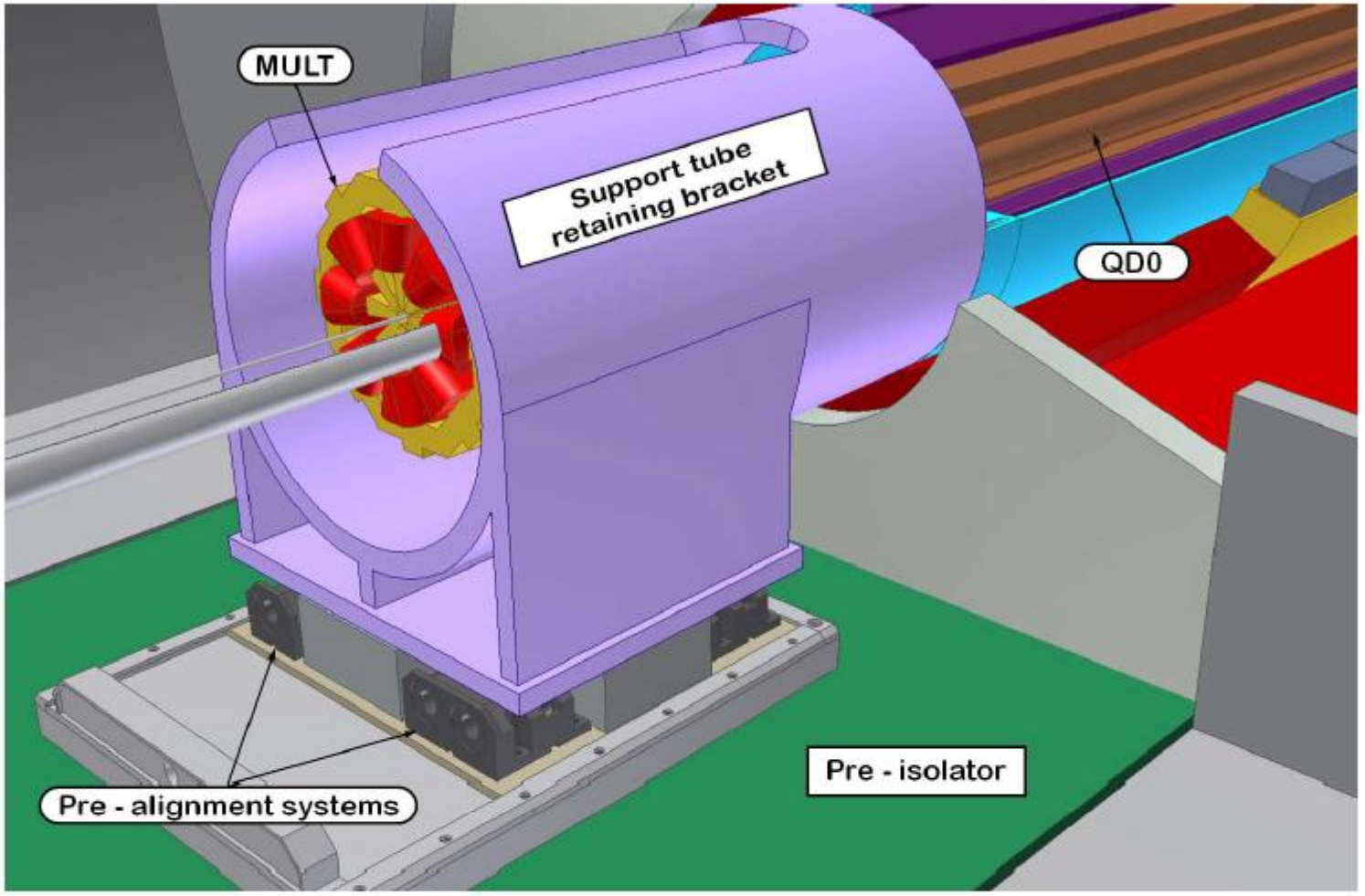

Fig. 11.14: Retaining bracket and pre-alignment underneath

Andre Sailer

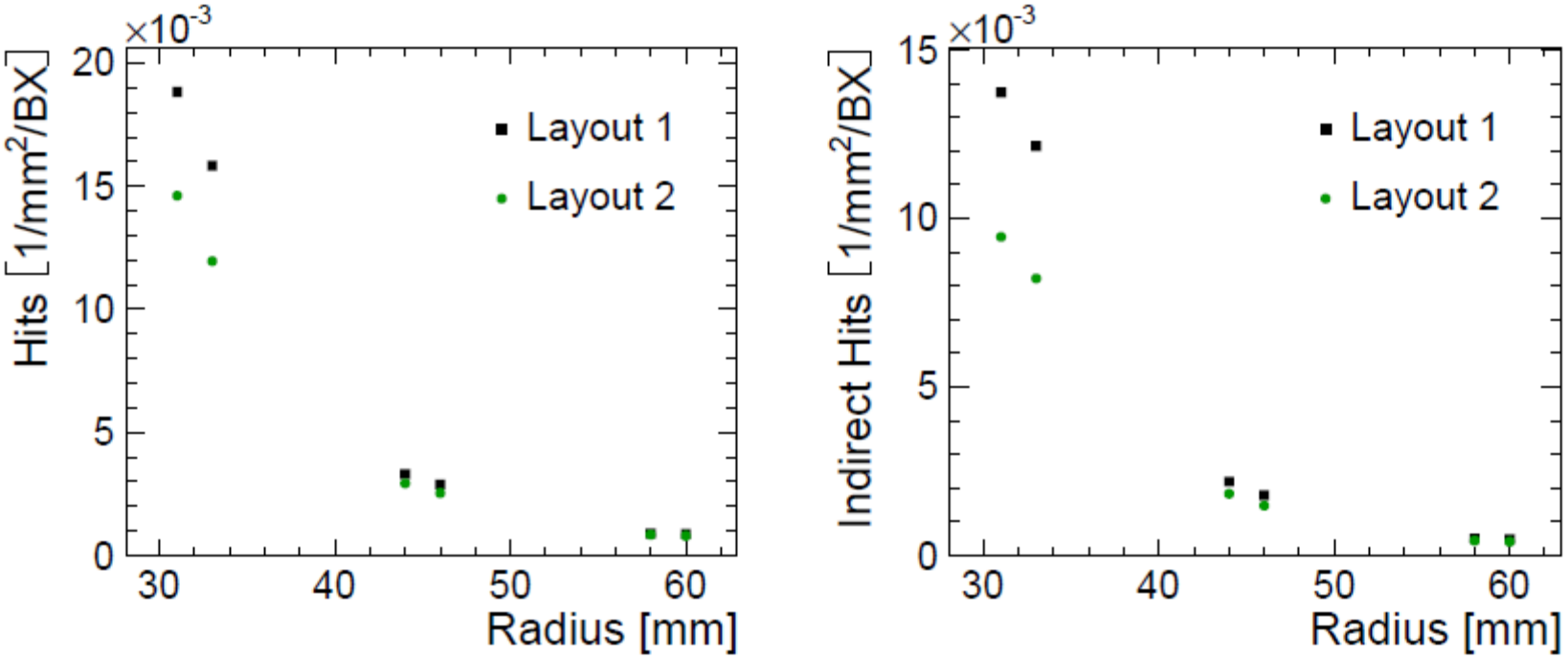

Fig. 9.2: Hit density in the different layers of the vertex detector for two different BeamCal cross sections (layout 1 and layout 2): all hits (left) and backscattered hits only (right).

Andre Sailer

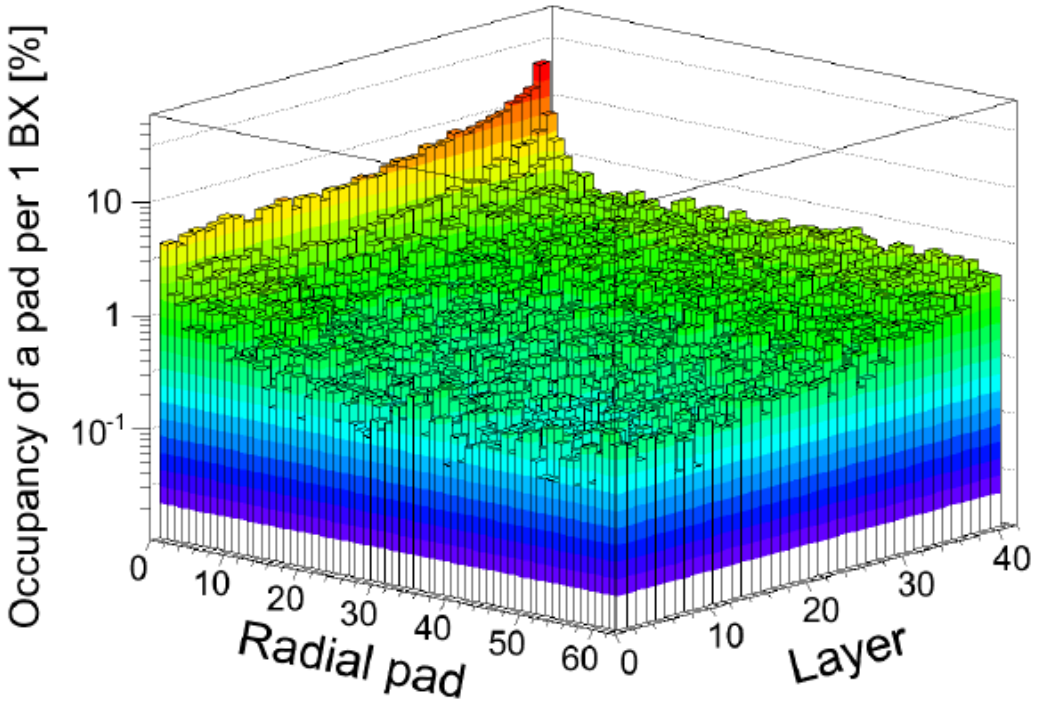

Fig. 9.4: Distribution of the occupancy per bunch crossing in each pad of the LumiCal due to incoherent pairs, averaged over 100 bunch crossings, as a function of the radial pad and sensor plane number. (Note that layer 1 is closest to the IP).

Andre Sailer

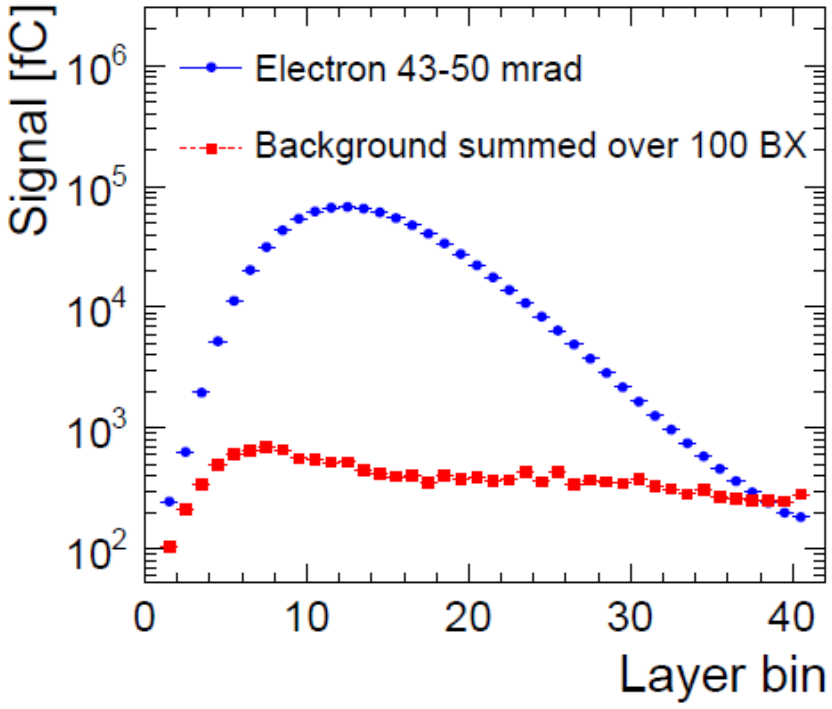

Fig. 9.5: Longitudinal profile of a 1.5 TeV electron shower, for electrons impacting the LumiCal in the angular range of 43 mrad to 50 mrad. Also shown is the expected contribution of the incoherent pairs background integrated over 100 bunch crossings.

Andre Sailer

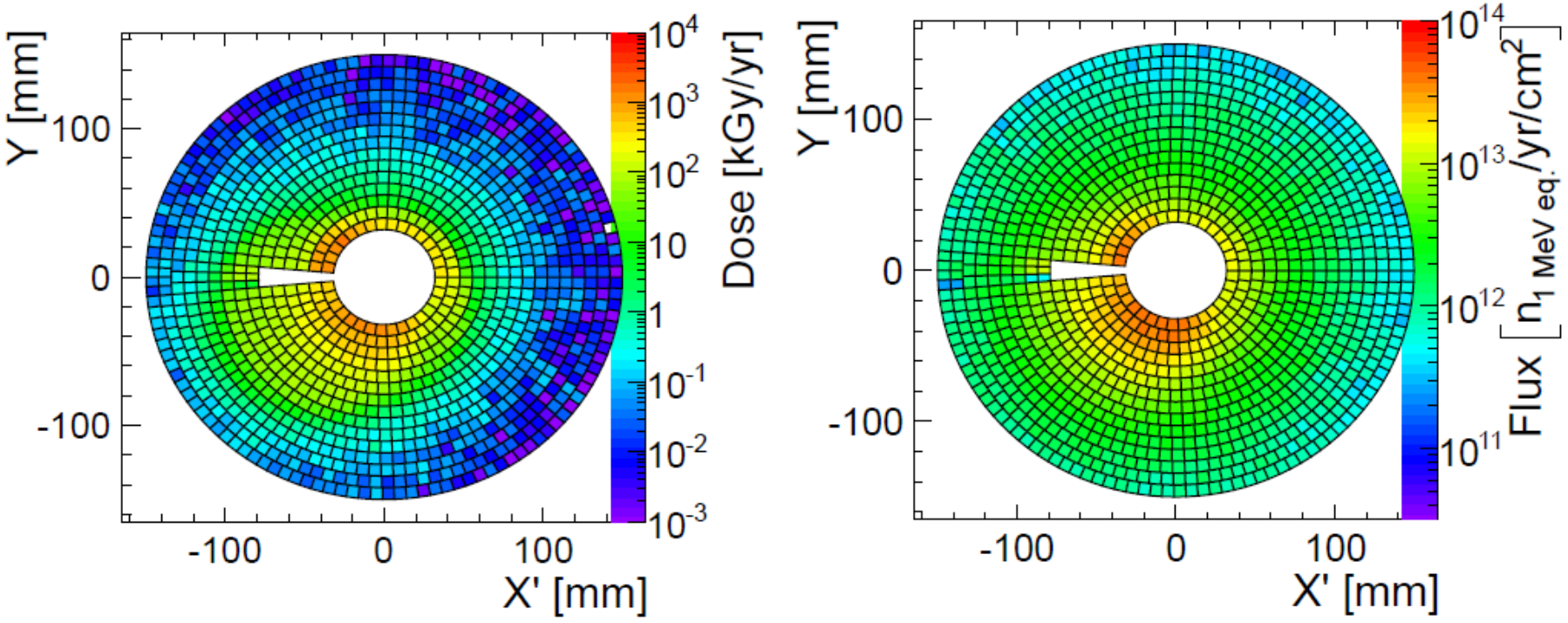

Fig. 9.7: The distribution of the expected total ionising dose (left) and 1 MeV equivalent neutron flux (right) per year in the fifth sensor layer of the BeamCal.

Since the time between bunch crossings is 0.5 ns and the duration of the bunch trains is only 156 ns, a trigger-less readout of the BeamCal and LumiCal after each train is envisaged. The occupancy in the BeamCal is very high, which calls for novel solutions in terms of readout electronics. One possibility for the readout is a gated integrator with correlated double sampling [1]. The charge collected in time slices of about 10 ns is either sampled by a fast ADC or stored in an analog memory and digitised after the bunch train. Between bunch trains, the integrator is reset. Signal amplitudes are obtained from subtracting subsequent samples. The subtraction would in addition serve as a noise filtering. This concept will also be applicable for the LumiCal.

The occupancy of the LumiCal estimated from simulations is below 2%. This allows to consider an alternative solution with a readout chain consisting of a fast preamplifier and shaper, followed by a fast digitiser. Finally, a deconvolution algorithm applied to the ADC output is being investigated [1]. From the deconvolution result the hit time and amplitude of the pad signals will be obtained. Further details on possible readout schemes are discussed in Chapter 10.

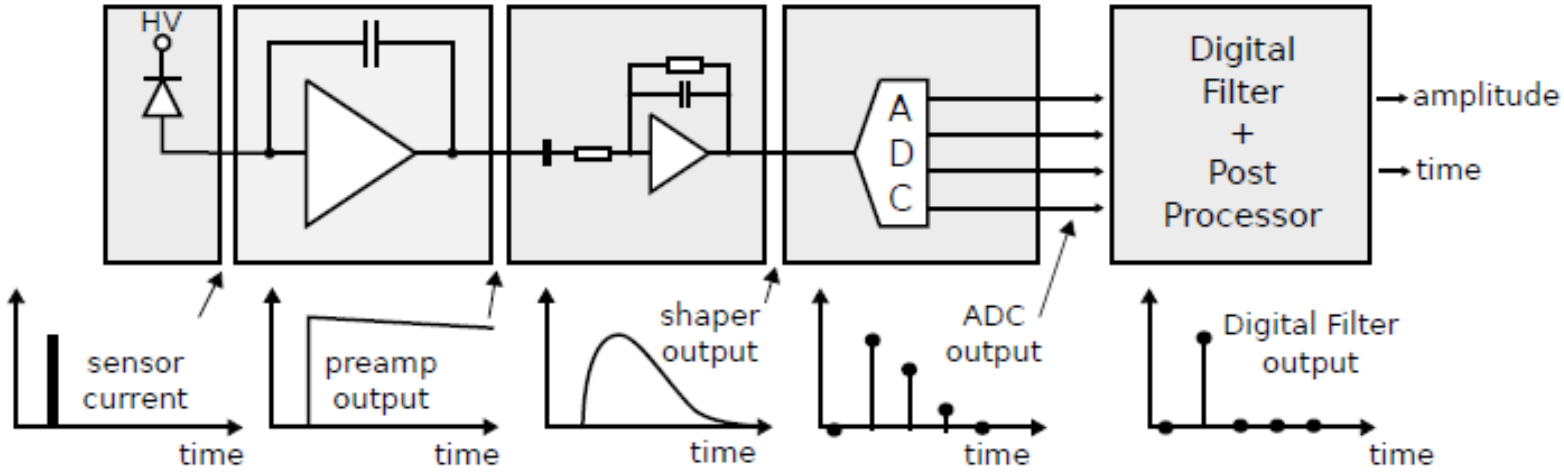

Fig. 10.1: Schematic view of proposed readout scheme for digital filtering. Figure taken from [18].

Spare Slides Part II (Pol.)

From CDR Vol. 1, DRAFT section on "Main Beam Injectors"

An electron source capable of producing spin-polarized electrons with a degree of polarization as high as 80%, GaAs-type cathodes as for example strained GaAs layer or InGaAs-AlGaAs super-lattice have been studied extensively around the world and are currently used at several accelerator laboratories [23], [24], [25]. These cathodes have demonstrated thousands of hours of lifetime under similar conditions as foreseen for CLIC.

0.1.4 Options for polarized positrons

As requested by the particle physics community an upgrade of CLIC to provide polarized positrons would be desirable at a certain point. Two main options have been studied and are described briefly below. The first option uses Compton backscattering of a polarized laser from an electron beam to generate polarized gamma-rays which then can be converted into polarized electron-positron pairs in a conversion target. The second schemes uses a helical undulator to produce directly polarized photons which are then converted into polarized positrons via a target. The feasibility of one of these options has not been demonstrated yet.

From CDR Vol. 1, DRAFT section on "Beam Delivery System"

The BDS is equipped with a polarization measurement station in the energy collimation section. Figure 2 shows the location of the polarization laser IP. At this location the beam travels parallel to the beam direction at the e^--e^+ IP and there is enough free space for the polarization laser. The backscattered electrons (or positrons) will deviate from the main beam trajectory thanks to the bending dipoles. These lower energy particles can be collected in a detector right before the energy spoiler. Excursions in the order of 100 mm are expected for particles loosing about 95% of the energy. With current existing laser technology the polarization measurement achieves a resolution better than 0.1% if averaging over 60 seconds.

Note: this is the ***statistical*** accuracy

The polarization laser collides with the beam with a 10 mrad angle. It should have a wavelength of 532 nm and an IP spot size of 50 μm. This set-up guarrantees a resolution of 0.1%.

How different is the depolarisation for different "slices" of the luminosity spectrum ?

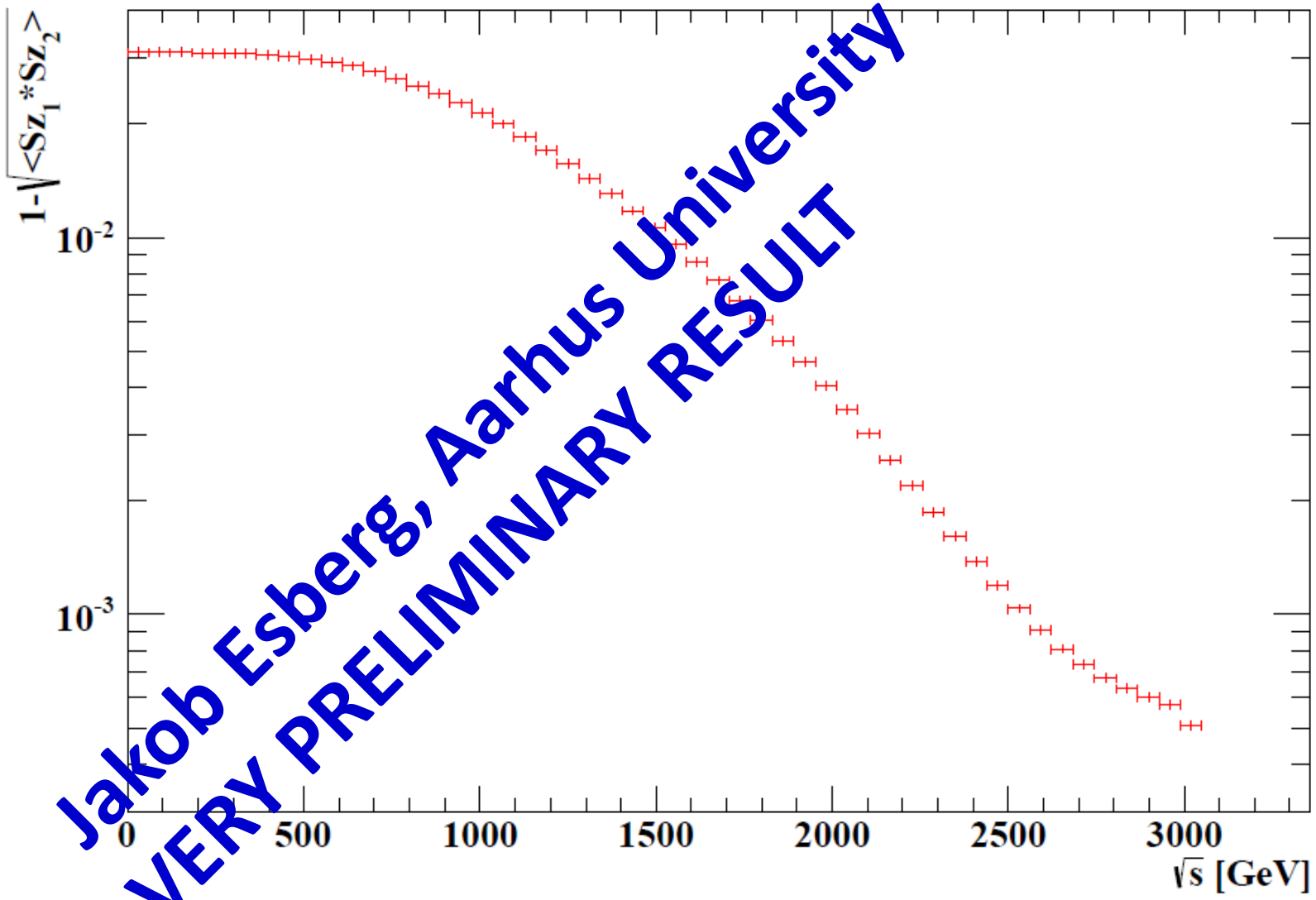

disrupted beam at interaction point

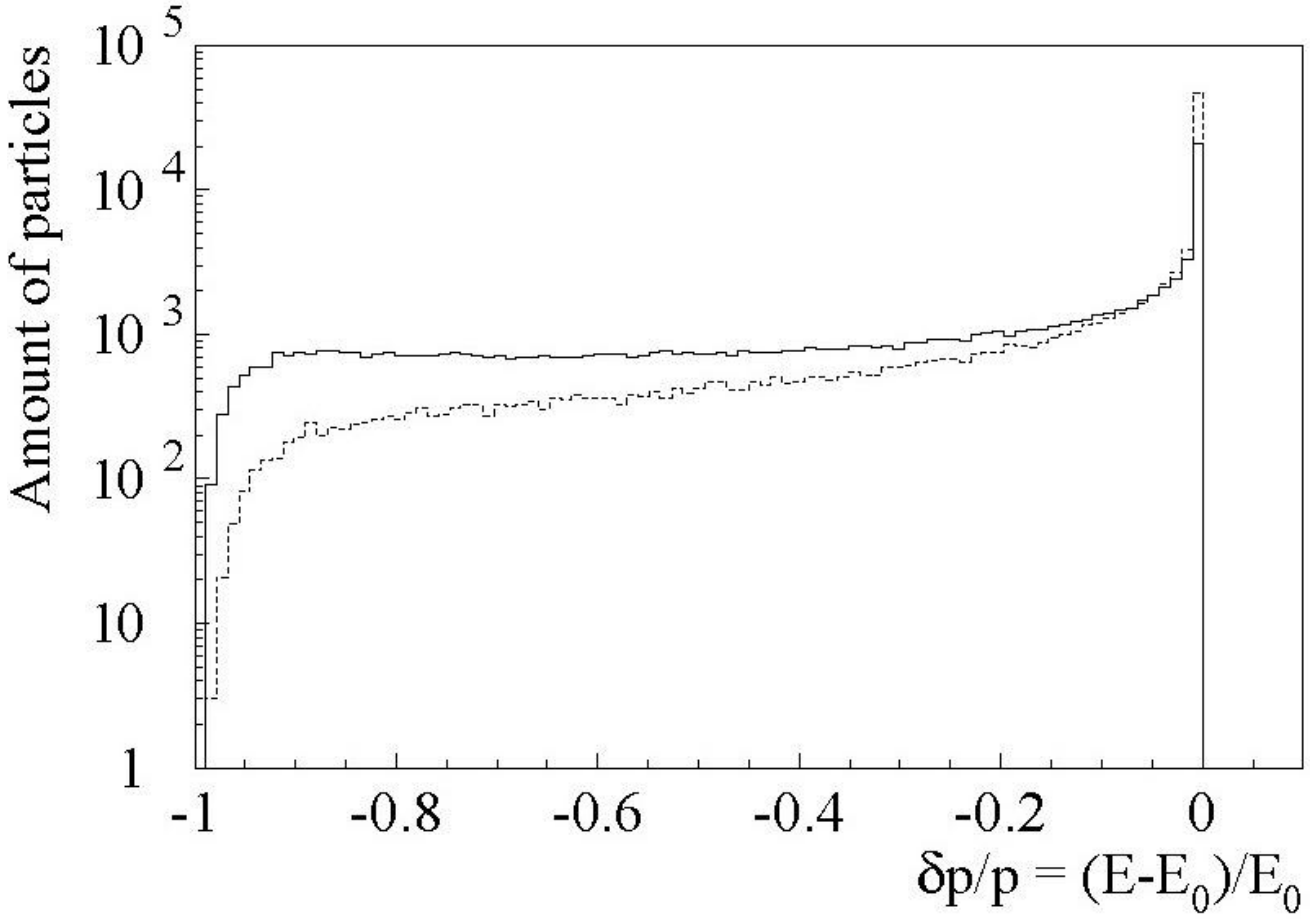

Arnaud Ferrari
EUROTEV-Report
2008-021

coherent pairs at interaction point

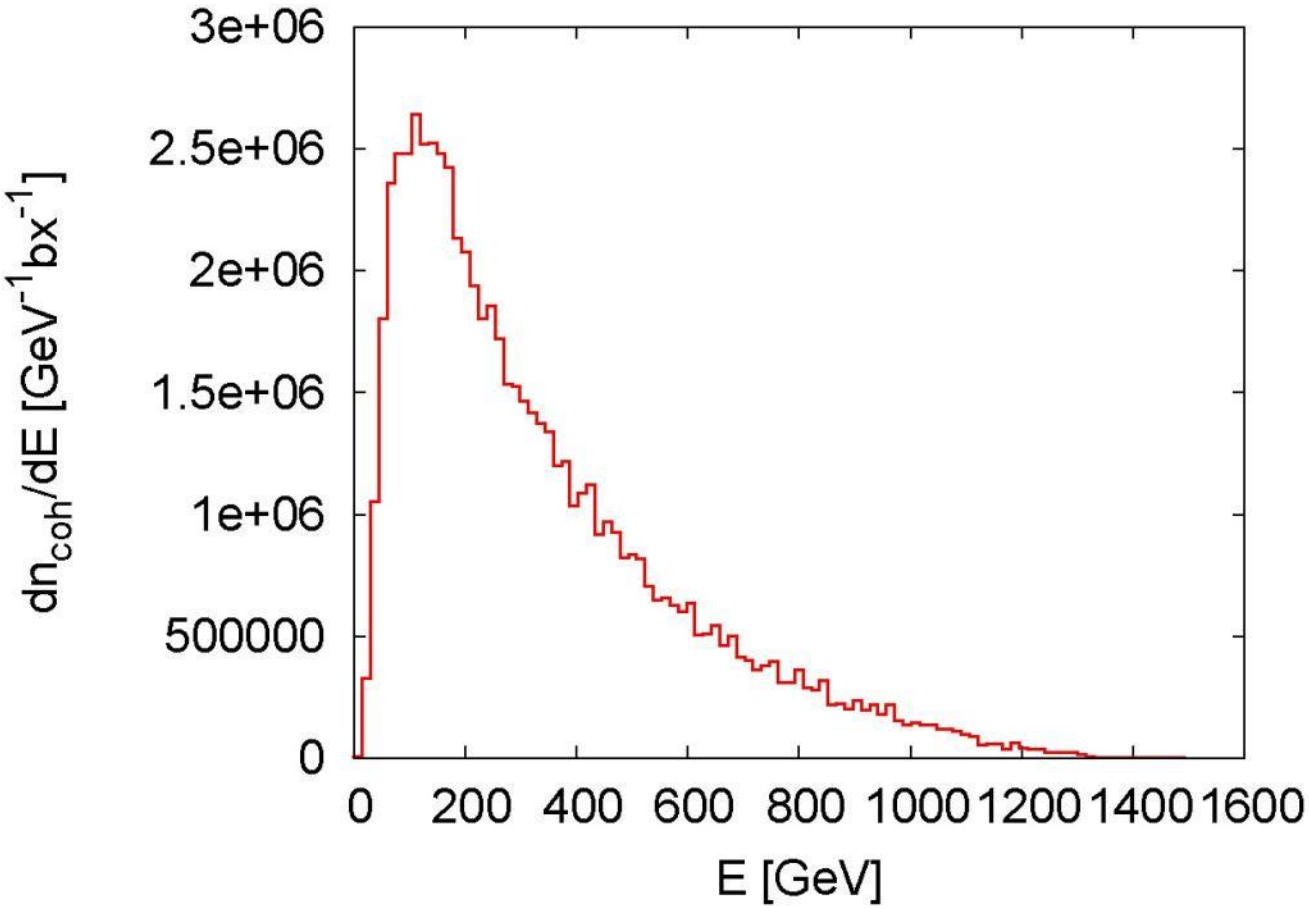

Daniel Schulte
Sendai, March 2008

Schematic of the CLIC post collision line (side view)

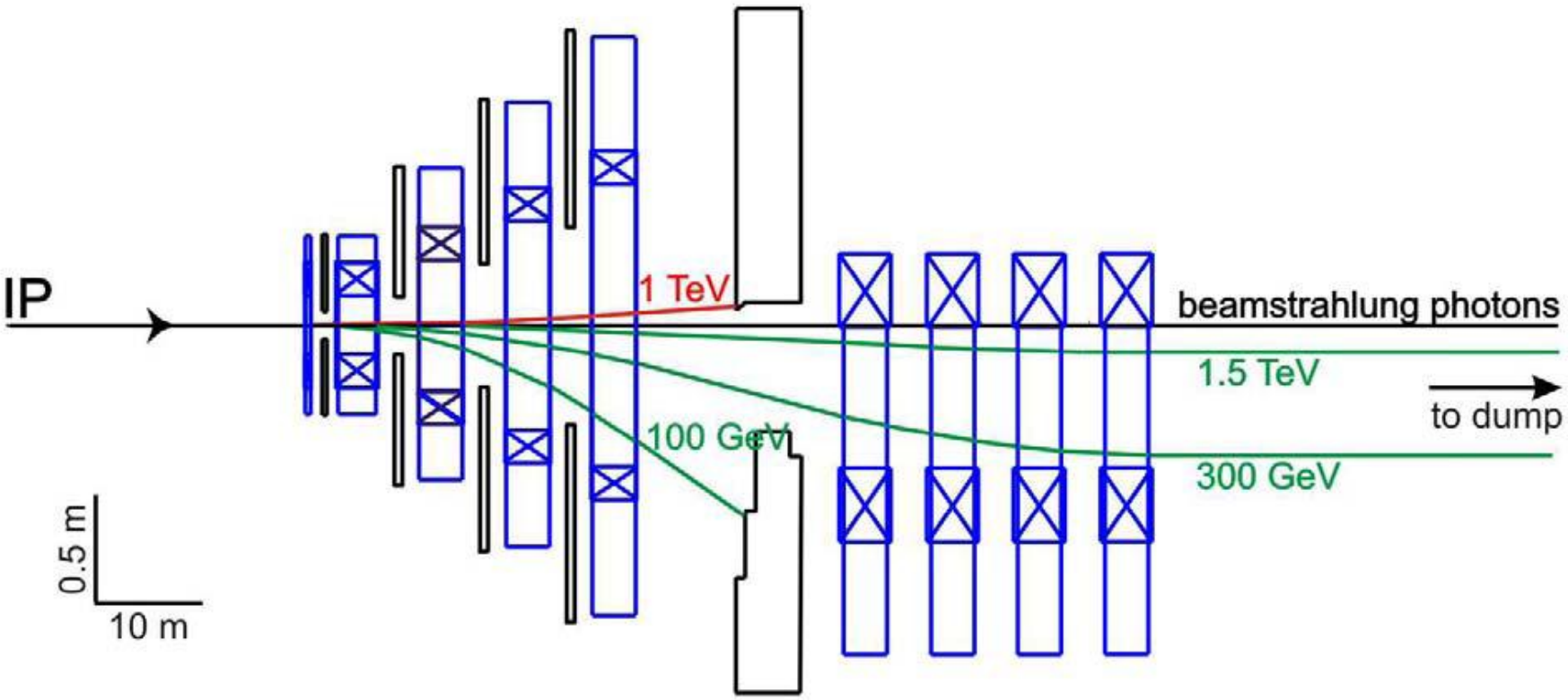

Particles after the Intermediate Dump of the PC line – nominal 3 TeV CLIC

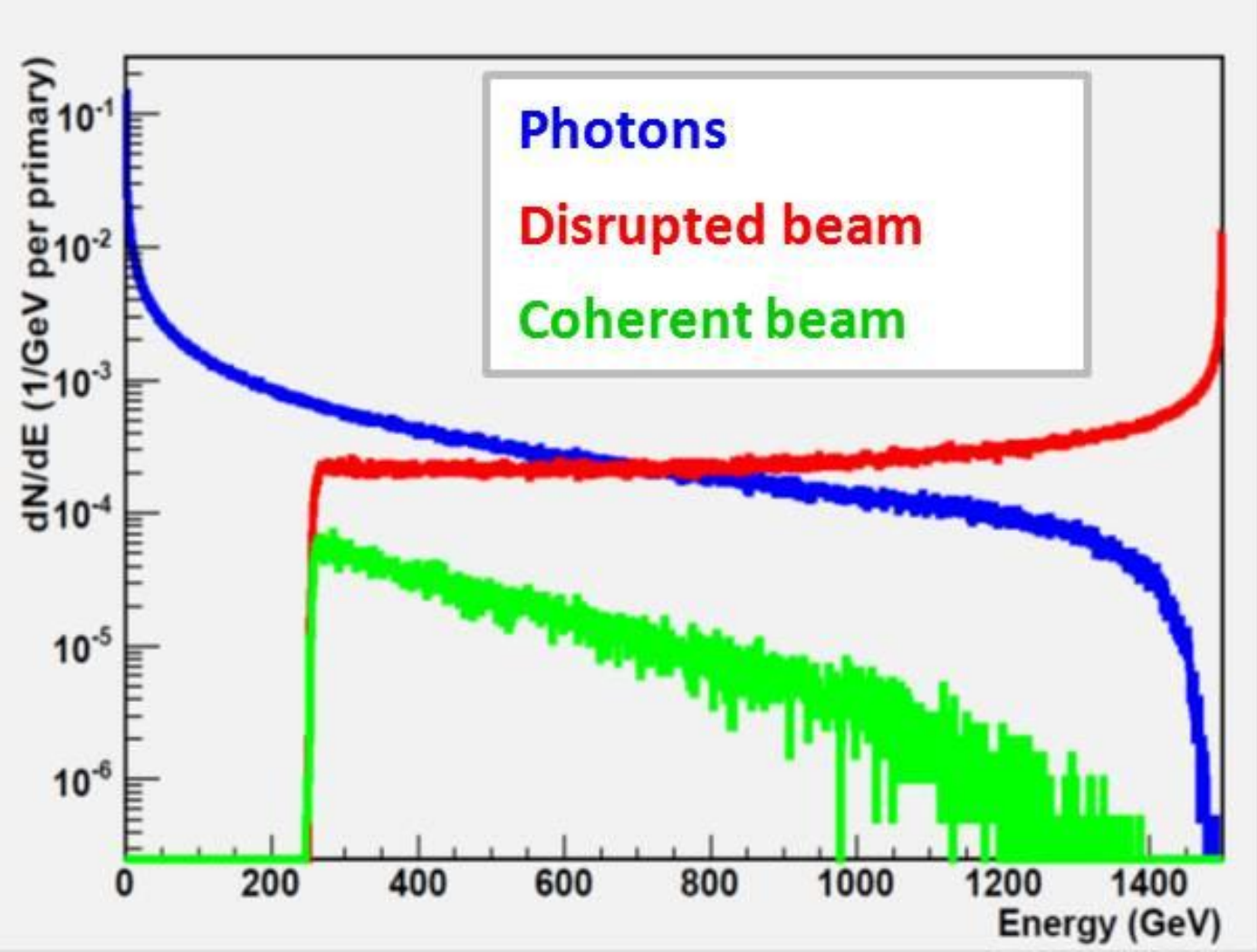

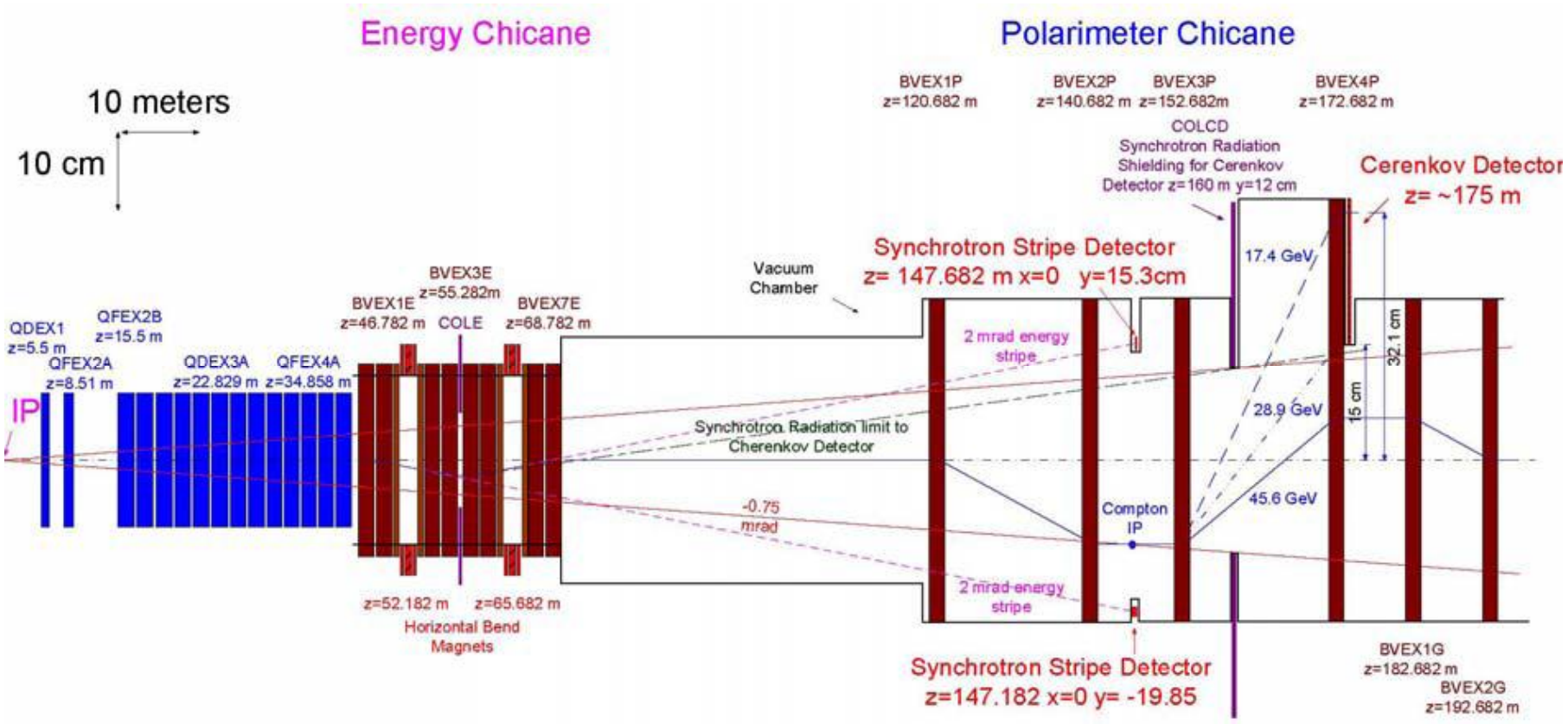
Energy Chicane
Polarimeter Chicane
10 meters
10 cm
BVEX1P
z=120.682 m
BVEX2P
z=140.682 m
BVEX3P
z=152.682m
BVEX4P
z=172.682 m
COLCD
Synchrotron Radiation
Shielding for Cerenkov
Detector z=160 m y=12 cm
Cerenkov Detector
z= ~175 m
Synchrotron Stripe Detector
z= 147.682 m x=0 y=15.3cm
Vacuum
Chamber
BVEX3E
z=55.282m
BVEX1E
z=46.782 m
COLE
BVEX7E
z=68.782 m
QDEX1
z=5.5 m
QFEX2B
z=15.5 m
QFEX2A
z=8.51 m
QDEX3A
z=22.829 m
QFEX4A
z=34.858 m
IP
2 mrad energy
stripe
17.4 GeV
32.1 cm
15 cm
28.9 GeV
Synchrotron Radiation limit to
Cherenkov Detector
-0.75
mrad
Compton
IP
45.6 GeV
2 mrad energy
stripe
z=52.182 m
z=65.682 m
Horizontal Bend
Magnets
Synchrotron Stripe Detector
z=147.182 x=0 y= -19.85
BVEX1G
z=182.682 m
BVEX2G
z=192.682 m

Spare Slides CDR Volume 1

from CDR Volume 1 (Accelerator)

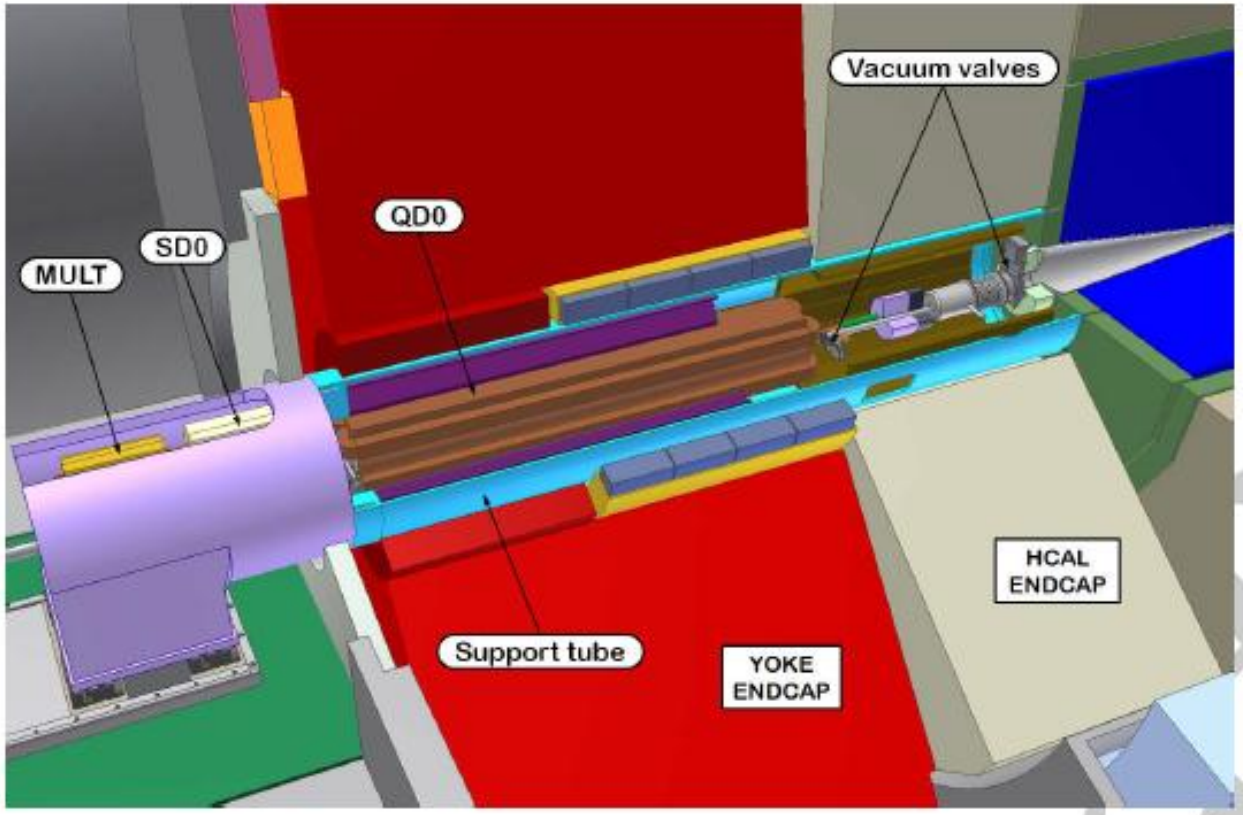

Fig. 3.11: MDI layout view (simplified). It shows in particular a representation of part of the final focus quadrupole QD0, integrated in the CLIC_SiD detector.

from CDR Volume 1 (Accelerator)

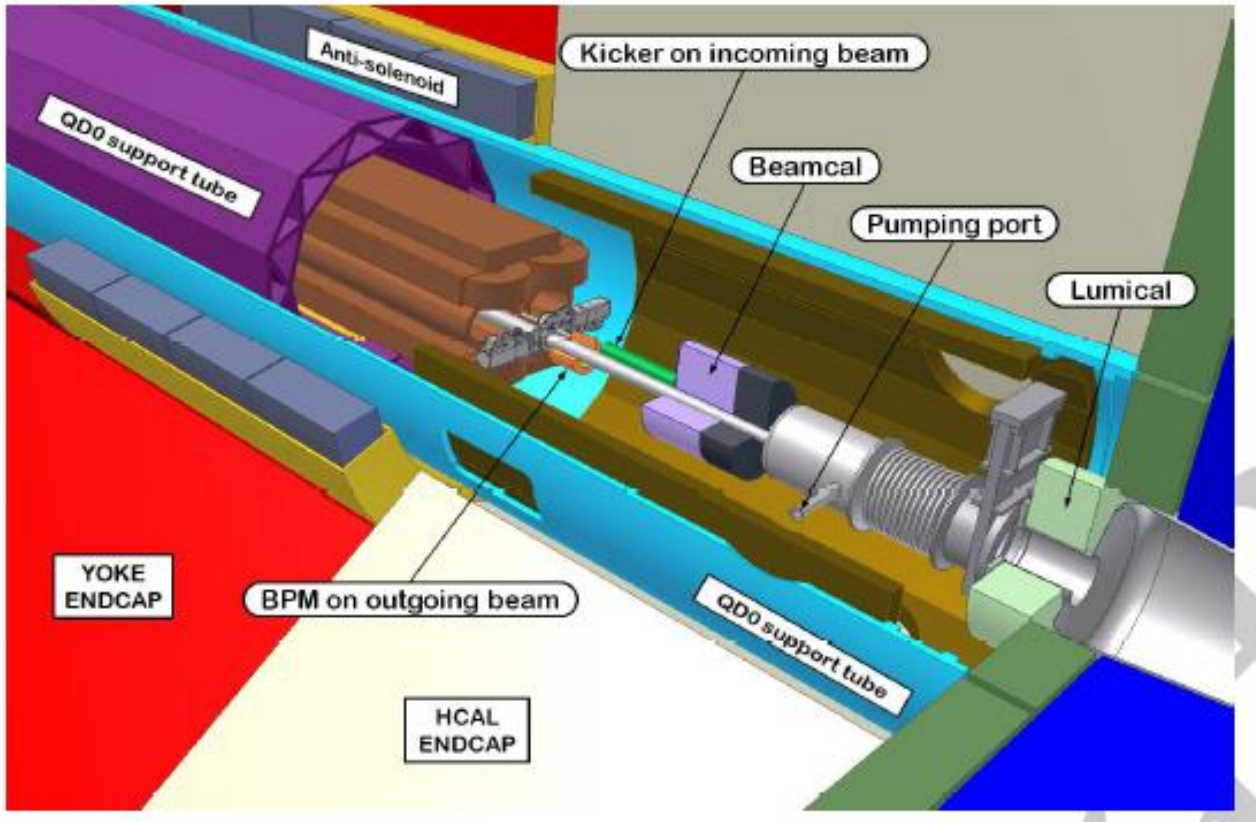

Fig. 3.12: Support tube concept in the MDI region.

from CDR Volume 1 (Accelerator)

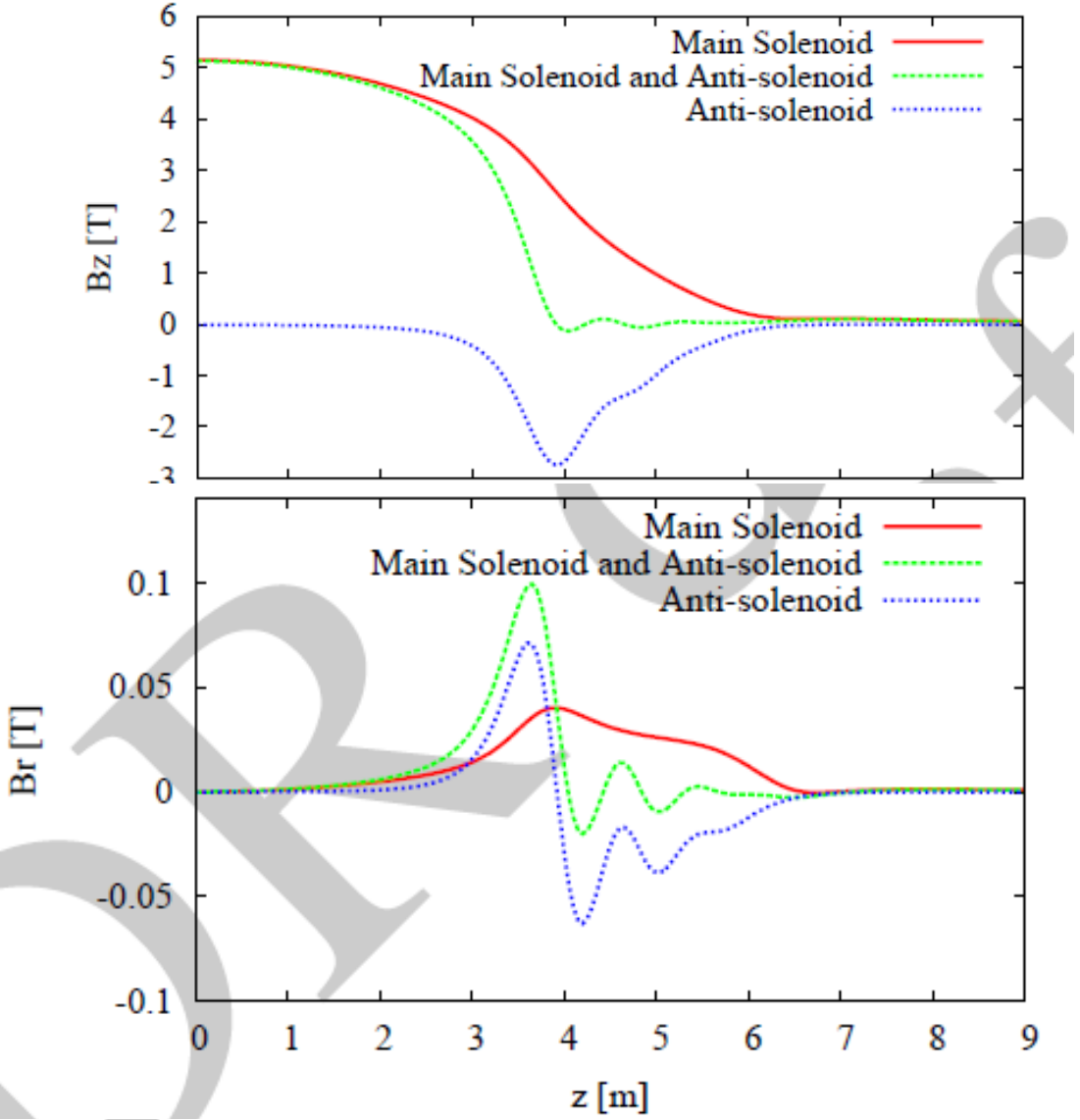

Fig. 3.13: The longitudinal field after compensation with the anti-solenoid is shown in (a), the radial field in (b), for the CLIC_SiD layout.

from CDR Volume 1 (Accelerator)

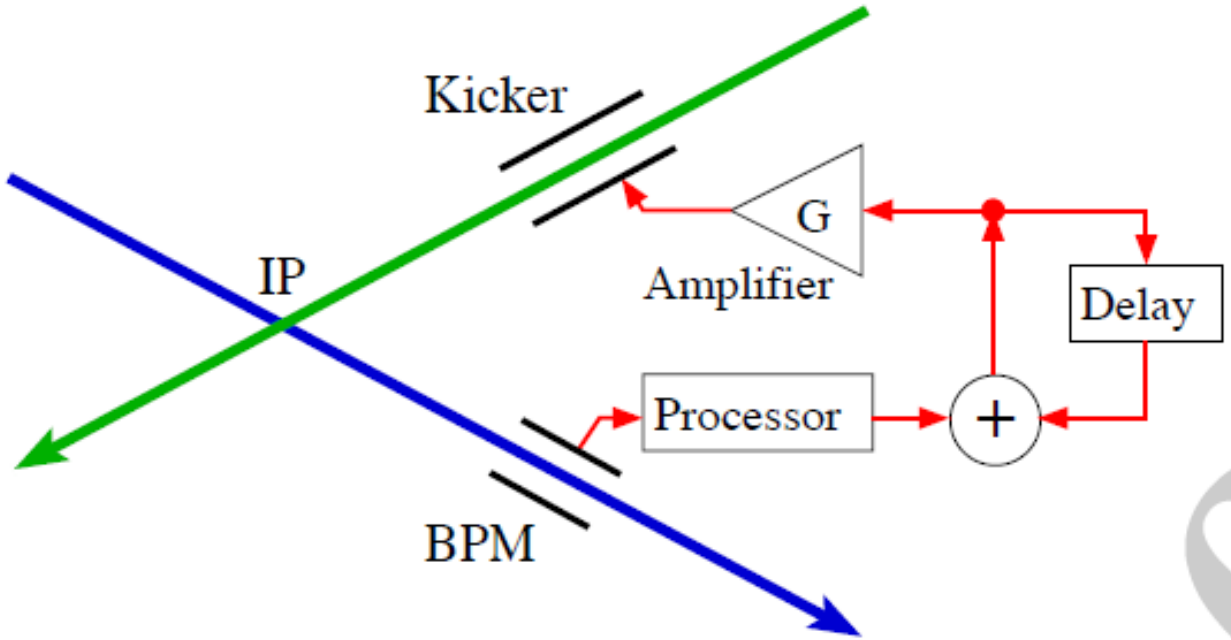

Fig. 5.74: Schematic layout of the IP feedback components.

from CDR Volume 1 (Accelerator)

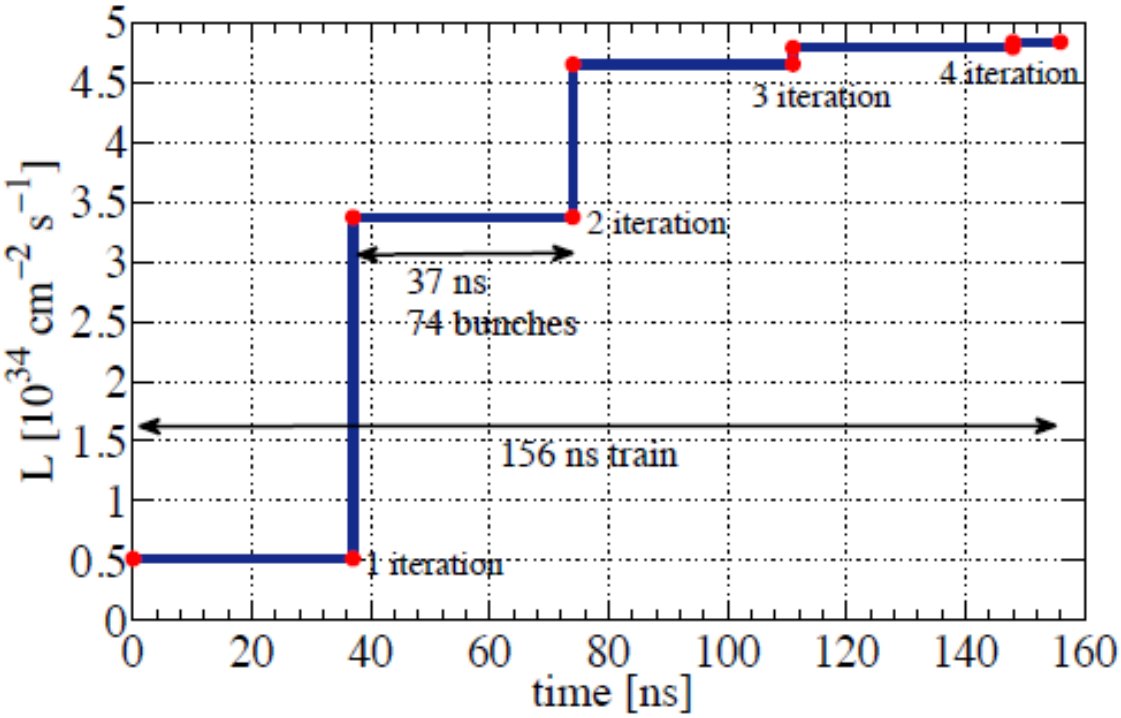

Fig. 3.14: Simulated luminosity versus bunch number for nominal CLIC 3 TeV parameters and assuming a noisy site for the ground motion.

from CDR Volume 1 (Accelerator)

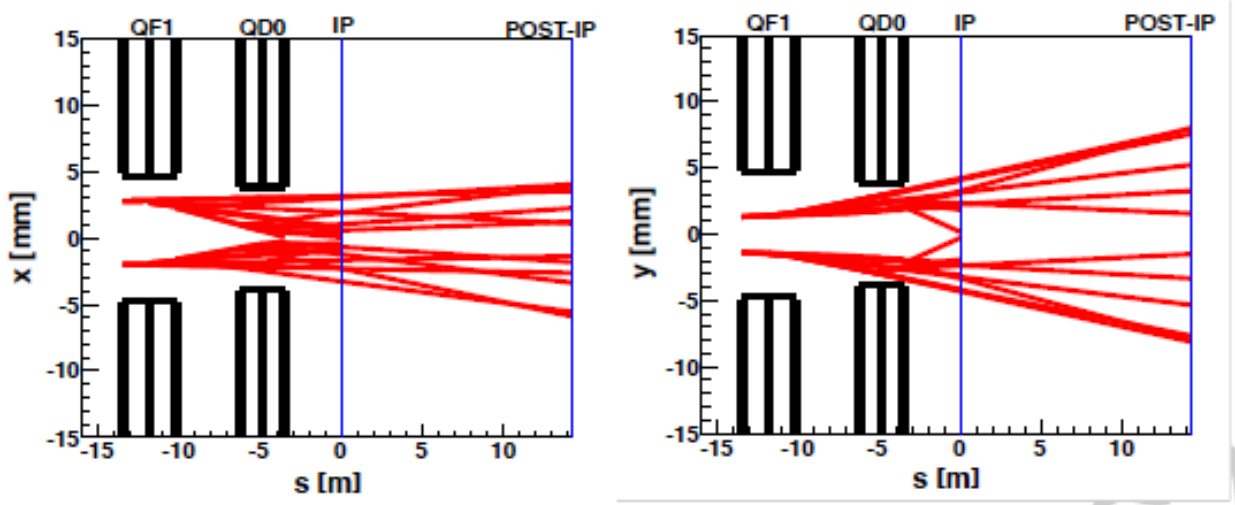

Fig. 3.16: Synchrotron radiation fans at 3 TeV centre-of-mass energy.

from CDR Volume 1 (Accelerator)

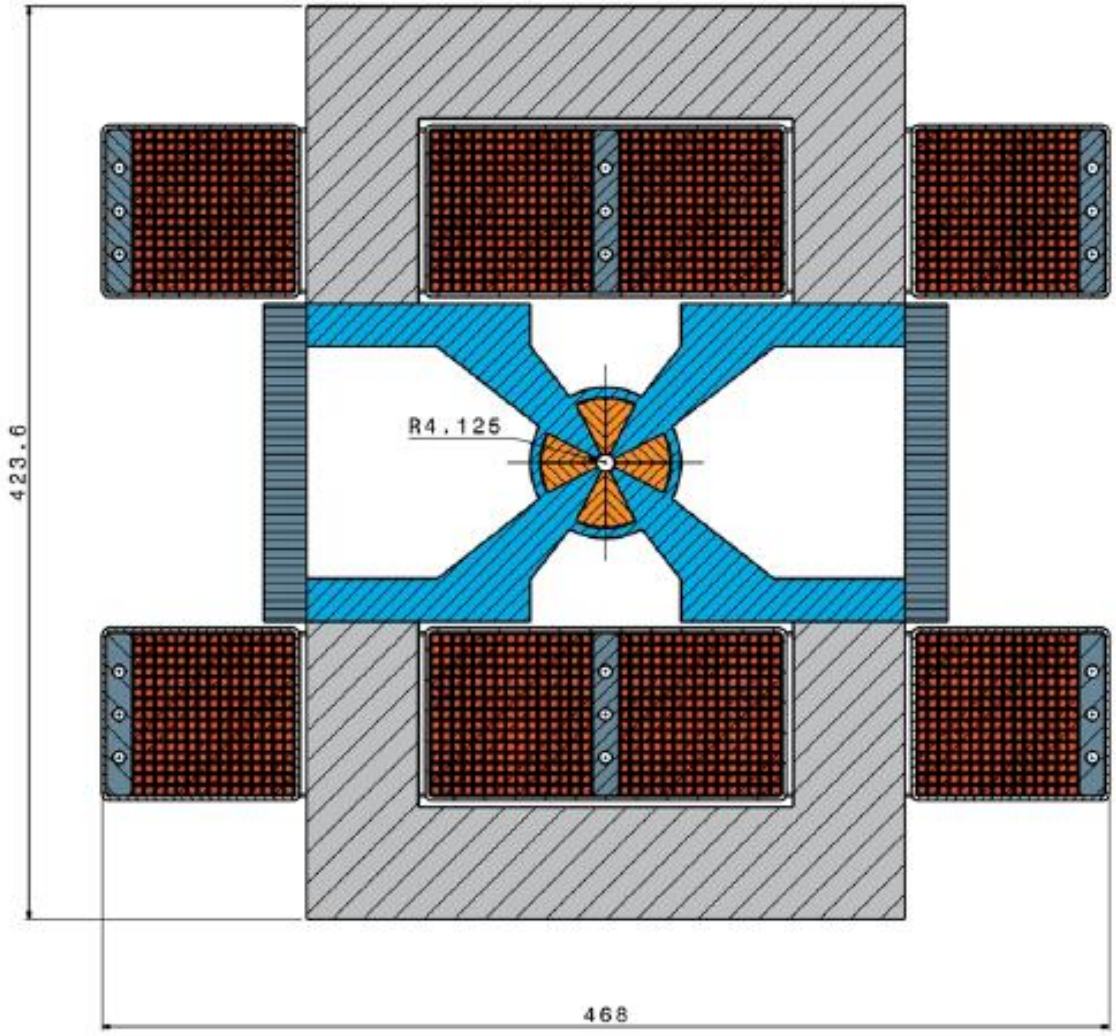

Fig. 5.61: QD0 with thermalization coils.

from CDR Volume 1 (Accelerator)

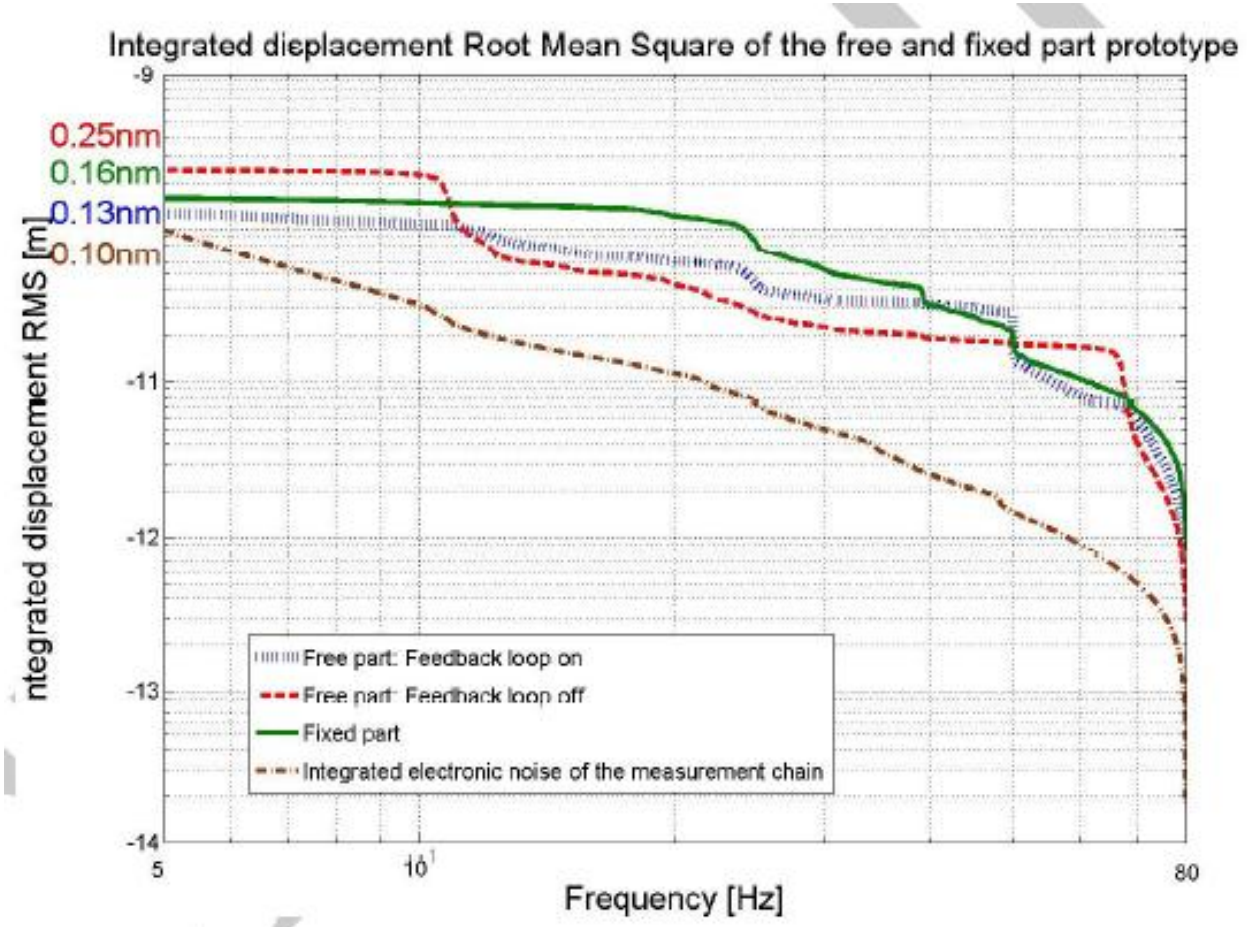

Fig. 5.64: Stabilization of a QD0 prototype to 0.13 nm for frequencies above 4 Hz.

from CDR Volume 1 (Accelerator)

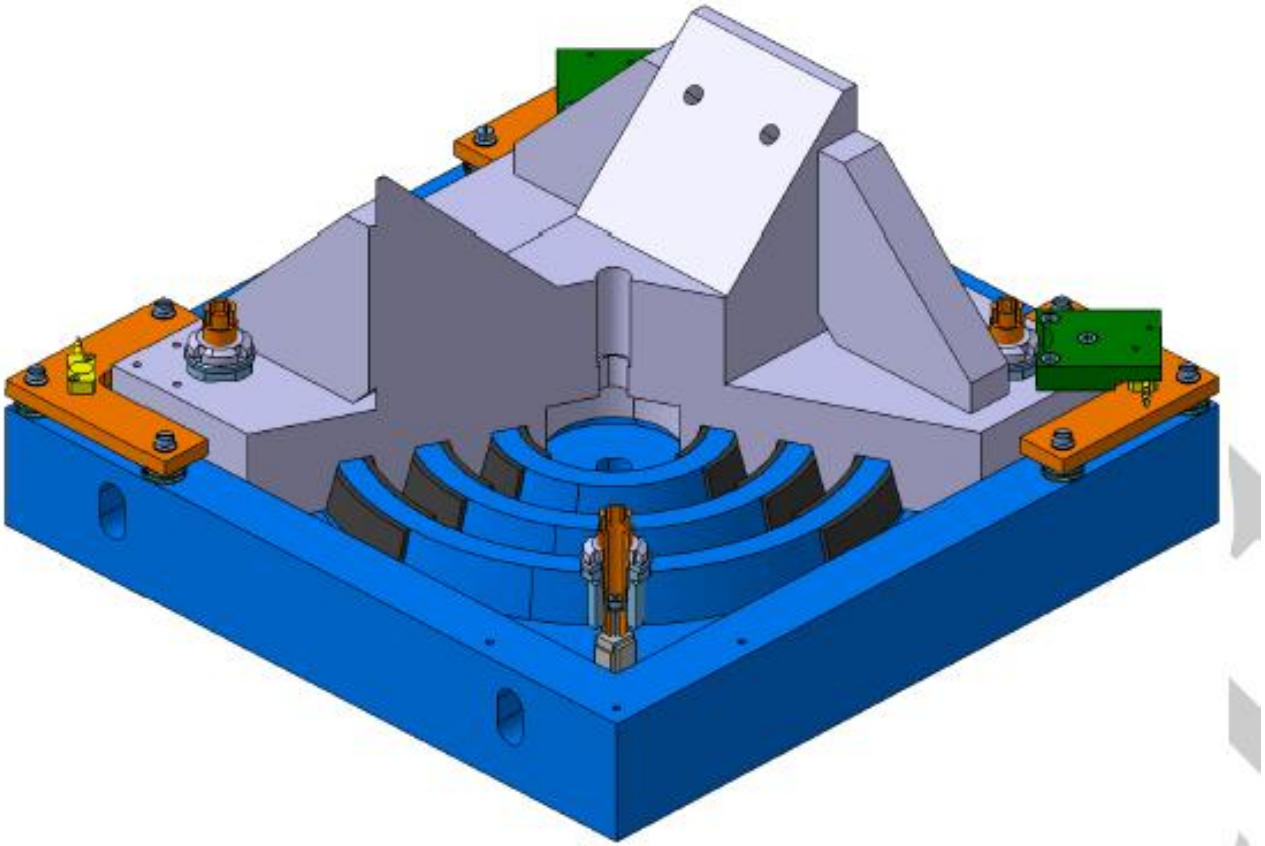

Fig. 5.65: Preliminary design of a stabilization device.

from CDR Volume 1 (Accelerator)

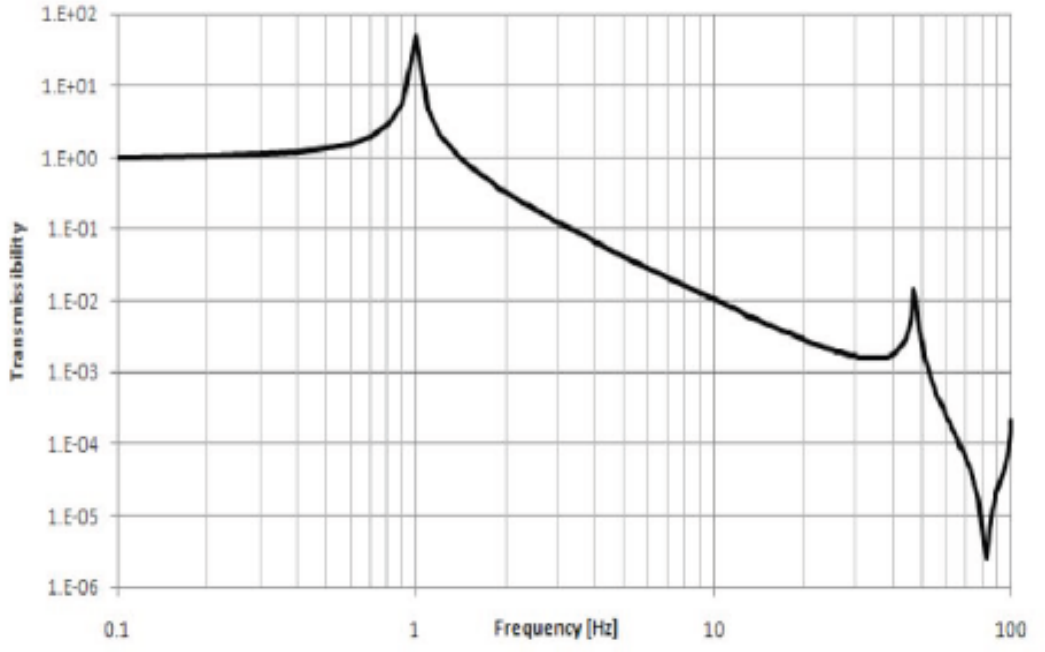

Fig. 5.67: Transfer function of a spring-mass system tuned at 1 Hz.

from CDR Volume 1 (Accelerator)

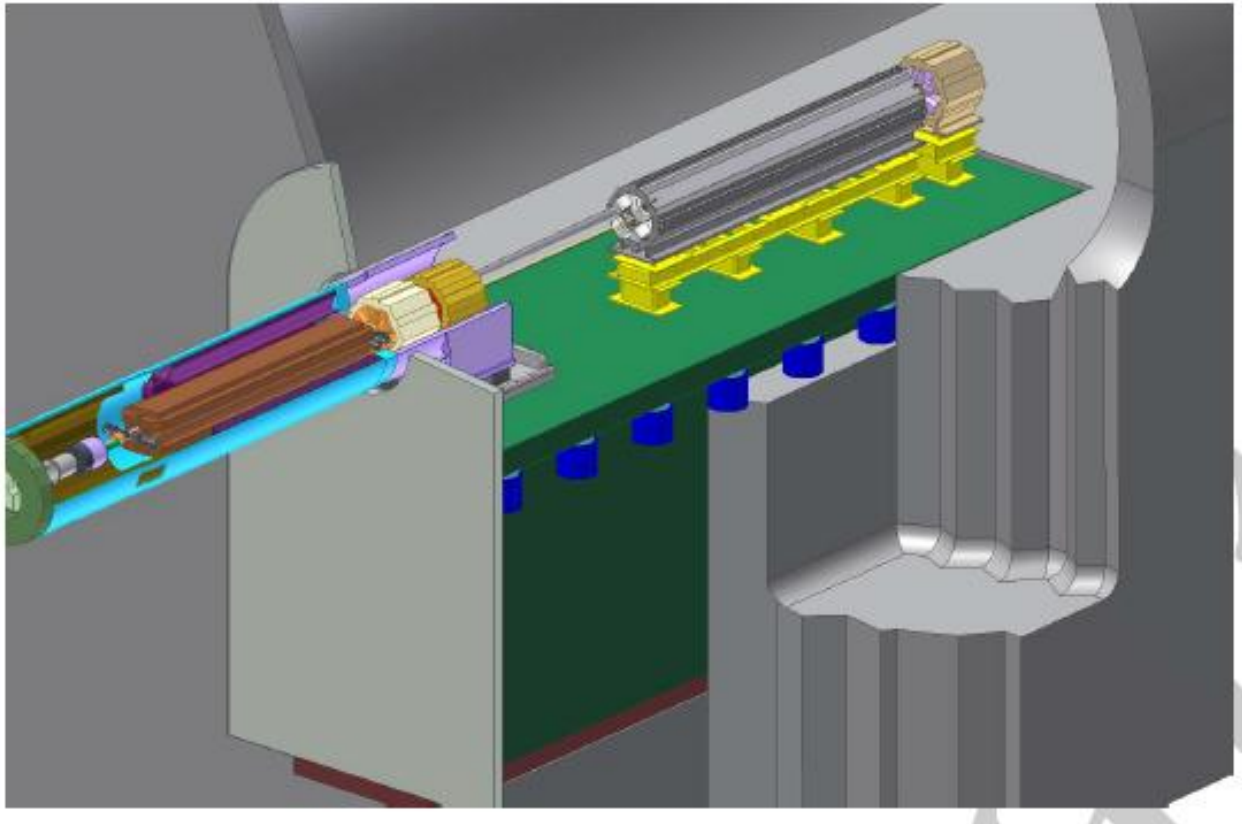

Fig. 5.68: Layout of the pre-isolator, with the concrete mass supporting the two final focus quadrupoles QD0 and QF1.

from CDR Volume 1 (Accelerator)

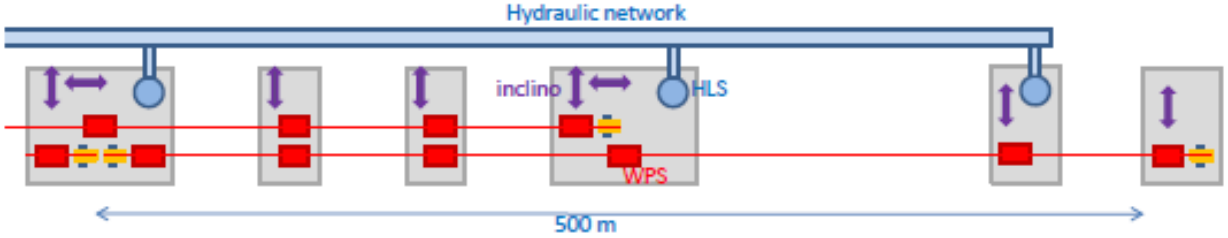

Fig. 5.69: Schematic layout of the pre-alignment equipment in the last 500 m of the tunnel.

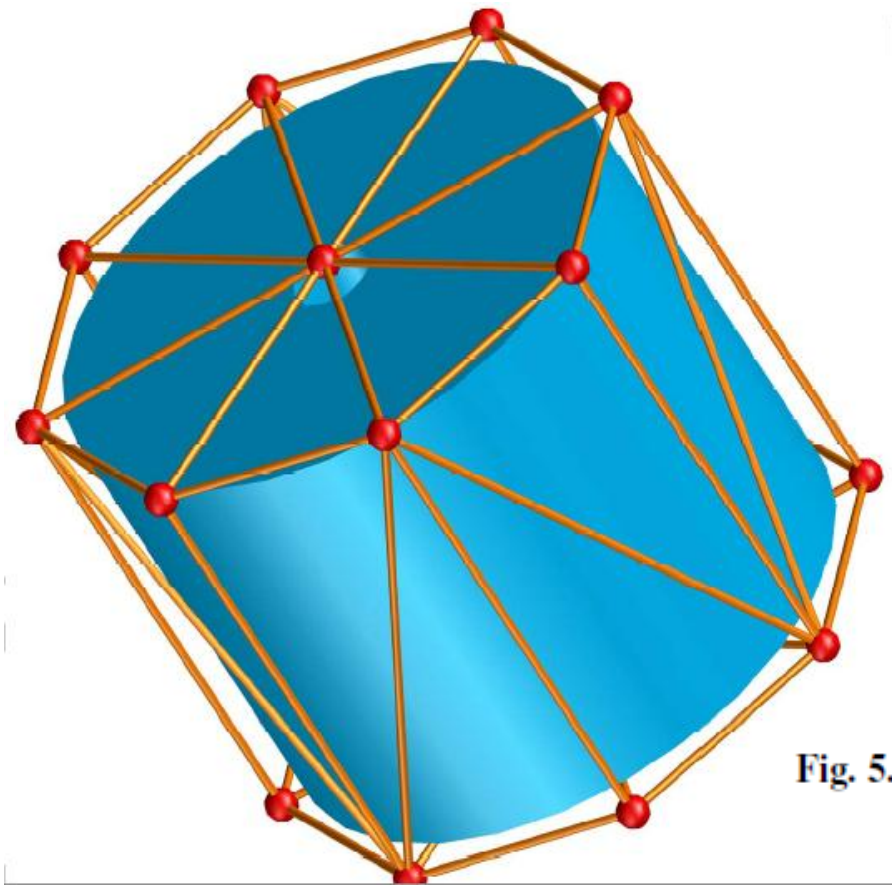

Fig. 5.70: Schematic layout of RASNIK nodes.

from CDR Volume 1 (Accelerator)

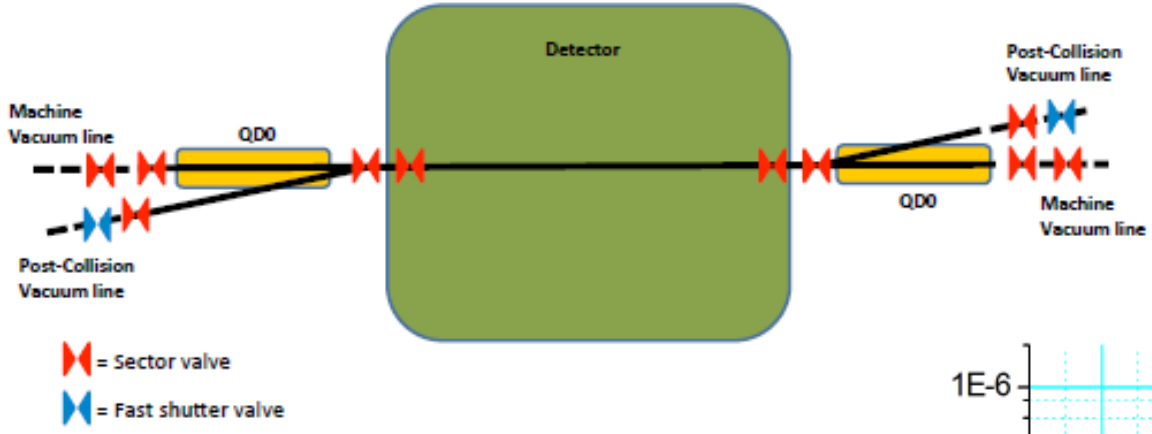

Fig. 5.77: Sectorisation of vacuum in MDI

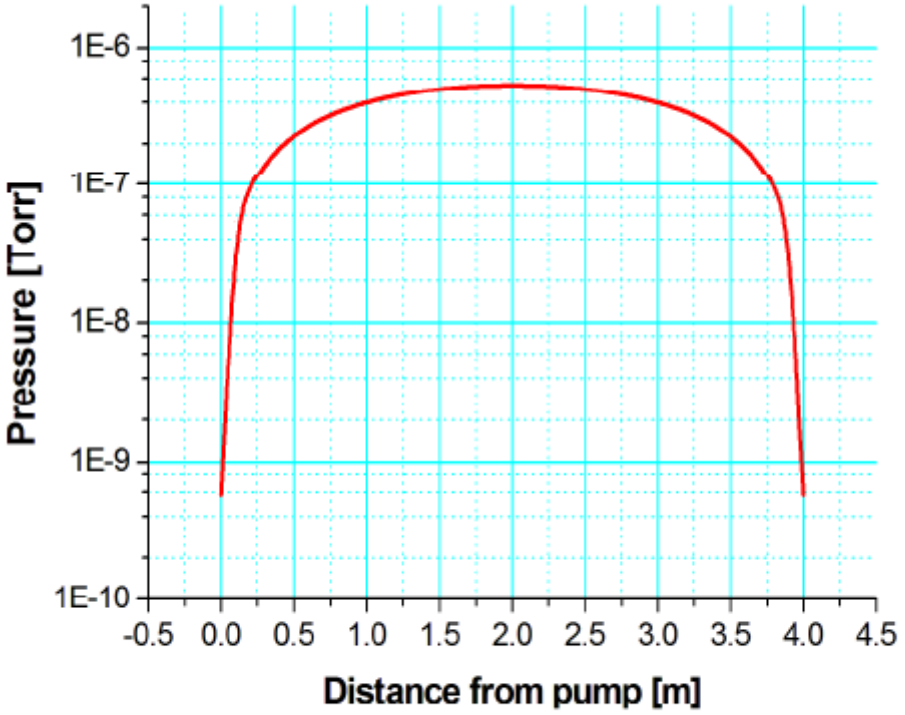

Fig. 5.76: Static pressure profile in QD0 region after 100 hours of pumping.